NASA TECHNICAL MEMORANDUM

NASA TM X-53755

August 6, 1968

NASA TM X-53755

AN EXPERIMENTAL STUDY OF THE BEHAVIOR OF A SLOSHING LIQUID SUBJECTED TO A SUDDEN REDUCTION IN ACCELERATION

By Louis E. Toole and Leon J. Hastings
Propulsion and Vehicle Engineering Laboratory

NASA

George C. Marshall Space Flight Center, Huntsville, Alabama

TECHNICAL MEMORANDUM X-53755

AN EXPERIMENTAL STUDY OF THE BEHAVIOR OF A SLOSHING LIQUID SUBJECTED TO A SUDDEN REDUCTION IN ACCELERATION

By

Louis E. Toole and Leon J. Hastings

George C. Marshall Space Flight Center
Huntsville, Alabama

ABSTRACT

The behavior of a liquid column oscillating in the fundamental antisymmetric mode and subjected to a sudden reduction in acceleration has been experimentally investigated. The amplitude and configuration of the liquid vapor interface, shifts in the liquid center of gravity, damping of the liquid motions, and the period of oscillation under the reduced gravity environment were examined using six-inch diameter scale model S-IVB LH_2 tanks. In addition, the effectiveness of a single ring baffle used as a propellant control device was evaluated.

NASA - GEORGE C. MARSHALL SPACE FLIGHT CENTER

NASA-GEORGE C. MARSHALL SPACE FLIGHT CENTER

TECHNICAL MEMORANDUM X- 53755

AN EXPERIMENTAL STUDY OF THE BEHAVIOR OF A SLOSHING LIQUID SUBJECTED TO A SUDDEN REDUCTION IN ACCELERATION

By

Louis E. Toole* and Leon J. Hastings

* Chrysler Corporation

PROPULSION DIVISION
PROPULSION AND VEHICLE ENGINEERING LABORATORY
RESEARCH AND DEVELOPMENT OPERATIONS

TABLE OF CONTENTS

LIST OF ILLUSTRATIONS

LIST OF ILLUSTRATIONS (Concluded)

LIST OF TABLES

DEFINITION OF SYMBOLS

Symbol	Definition	Units
a	Local acceleration	ft/sec^2
B_o	Bond number	
d	Distance from liquid surface to baffle	ft
E	Total energy	$ft\text{-}lb_f$
f	Liquid frequency	cps
F_r	Froude number	
g_c	Dimension constant	$32.2\ lb_m ft/lb_f sec^2$
g_o	Standard gravitational acceleration	ft/sec^2
h	Nominal liquid depth above bottom of container	ft
H	Vertical distance between two liquid-vapor interfaces, $Z_1(x) - Z_2(x)$	inches
L	Semi-chord length of a circular arc	inches
m_s	Sloshing mass	lb_m
M	Volume moment	$inches^4$
P	Period of wave motion	seconds
P.E.	Potential energy	$ft\text{-}lb_f$
r	Radius of curvature of liquid-vapor interface in the yz plane	inches
R	Container radius	ft, in.
t	Time	seconds
v	Volume	$inches^3$
V	Velocity	ft/sec
w	Baffle width	ft
x, y, z	Rectangular Coordinates	
Z(x)	Polynominal description of the liquid-vapor interface in the xz plane	

DEFINITION OF SYMBOLS (Concluded)

Symbol	Description	Units
Z_{min}	Distance from the nominal liquid level to the lowest point on the liquid-vapor interface when the interface is at maximum amplitude	inches
β	Kinematic surface tension, $\sigma g_c/\rho$	ft^3/sec^2
Δ	Incremental dimension	
δ	Logarithmic decrement	
ζ	Maximum liquid amplitude	ft
θ	Contact angle	degrees
ν	Kinematic viscosity	ft^2/sec
ρ	Density	lb_m/ft^3
σ	Surface tension	lb_f/ft
ϕ	Wave phase angle	degrees
ω	Liquid circular frequency	radians/sec

SUBSCRIPTS

a	Average
f	Final
h	High gravity conditions
i	Initial
ℓ	Low gravity conditions

AN EXPERIMENTAL STUDY OF THE BEHAVIOR OF A SLOSHING LIQUID SUBJECTED TO A SUDDEN REDUCTION IN ACCELERATION

SUMMARY

The behavior of a liquid column oscillating in the fundamental antisymmetric mode and subjected to a sudden reduction in axial acceleration has been experimentally investigated. The Marshall Space Flight Center drop tower facility was used to obtain a controlled low gravity environment for durations of up to 4.3 seconds. Tests were conducted in six-inch diameter cylinders using petroleum ether, a zero contact angle liquid, as the test fluid. The test conditions provided Bond numbers and Froude numbers, based on tank radius (R), ranging from 12 to 100 and about .03 to 22, respectively. Engineering results were obtained that have general application in the design of propellant control systems. In addition, the liquid behavior for the specific S-IVB-203 geometric configuration and energy conditions at orbital insertion, both with and without the baffle and deflector installed, was evaluated.

The results indicated that, for measured Froude numbers from .03 to 14.6 in combination with Bond numbers from 24 to 100, the maximum liquid amplitude is uniquely dependent on the Froude number. Simulation of the unbaffled S-IVB-203 LH_2 energy conditions (Froude number = 19.3) produced amplification of the slosh wave to the top of the forward dome of the model S-IVB LH_2 tank for two successive slosh cycles in the low gravity environment. A ring baffle positioned either at or slightly above the liquid surface was highly effective in reducing slosh wave amplification and damping the low gravity liquid motion. The nature of the liquid behavior in model tests of the S-IVB-203 configuration was strikingly similar to that observed on the AS-203 flight after orbital insertion.

The logarithmic decrement describing the decay of the amplitude of oscillation in a low gravity environment due to viscous dissipation when the initial amplitude is between 0.6 R and 1.05 R was found to be amplitude dependent and to increase with increasing amplitude. Initial damping for large amplitude sloshing is considerably higher than predicted by available correlations. The frequency of oscillation of the liquid column shifts instantaneously with changes in the applied acceleration. The measured wave period of the first cycle of motion following a reduction in acceleration was found to agree with the Satterlee-Reynolds equation within ± 8 percent at all Bond numbers within the range obtained in this program. Empirical equations were developed for determining the maximum shift in liquid center of gravity as a function of Froude number for liquid depths of 1.0 R or greater.

INTRODUCTION

One of the basic engineering problems in the design of space vehicles is the control or proper positioning of the liquid propellants. Many missions, such as the Saturn V lunar mission, will require an extended low gravity orbital coast period with a subsequent restart of the main propulsion engine. Proper orientation of the liquid propellants during the coast period is necessary for satisfactory functioning of the propellant tank vent system for the operation of the engine thermal conditioning systems prior to restart. In addition, propellant control is essential for minimizing disturbances to the vehicle that could impose excessive demands on the attitude control system.

An especially severe propellant control problem can exist immediately following main engine cutoff. Liquid sloshing amplitudes that are relatively small during the high-g conditions of powered flight may attain very large amplitudes following engine shutdown when the liquid kinetic energy is converted into potential energy in the reduced gravity field. In fact, slosh wave amplification was a foremost concern in the design of the Saturn V/S-IVB stage propellant control system and became a significant factor in the decision by NASA to perform the full-scale AS-203 Low Gravity LH_2 Experiment using a Saturn IB/S-IVB stage to simulate the earth orbital phase of the Saturn lunar mission.

Prior to the AS-203 flight the Marshall Space Flight Center initiated an experimental program to study the various low gravity problems associated with the Saturn V lunar mission, with initial emphasis on the AS-203 LH_2 experiment. The program is being conducted in the MSFC 4.3-second drop tower facility. One phase of the experimental program was an investigation of the behavior of a sloshing liquid subjected to a sudden reduction in acceleration. This report discusses the results from that phase of the program.

The basic objectives of the program were to (1) evaluate the liquid behavior for the specific S-IVB-203 geometric configuration and energy conditions--both with and without the baffle and deflector installed, (2) assess the effectiveness of slosh baffles as propellant control devices, and (3) obtain quantitative data applicable to the design of any cylindrical propellant containers. The amplitude and configuration of the liquid-vapor interface, shifts in the propellant center of gravity, damping of the liquid motions, and the frequency of oscillation under the reduced gravity conditions were of concern from an engineering design standpoint.

Fluid behavior during the low gravity period provided by the drop tower was recorded using high speed photography (approximately 400 frames/second). A motion picture supplement to this report was prepared and is available on loan. The 16 mm, 11 minute film, Number M-281 can be obtained from:

Photographic Branch T5-P
Marshall Space Flight Center
Redstone Arsenal, Alabama
35812

This report was prepared by Chrysler Corporation and Marshall Space Flight Center under the technical supervision of Leon J. Hastings, Fluid Mechanics Section, Propulsion and Vehicle Engineering Laboratory, George C. Marshall Space Flight Center, under Contract NAS-8 4016, Schedule II, Modification 292, change order MSFC-1, Amendment 39.

BACKGROUND

Scaling Parameters

Space vehicle acceleration histories typically vary from values higher than one-g during powered flight to accelerations on the order of only 10^{-5} or 10^{-6} g's during orbital operations. Liquid containers may range from one foot in diameter to greater than 20 feet. To permit reliable extrapolation from model test results to full-scale vehicle and spacecraft systems, appropriate dimensionless parameters are employed. The Bond number and the Froude number are the scaling parameters applicable to the problem discussed in this report where

$$\text{Bond number, } B_o = \frac{\text{gravitational force}}{\text{capillary force}} = \frac{\rho R^3 a/g_c}{\sigma R} = \frac{R^2 a}{\beta} \qquad (1)$$

$$\text{Froude number, } F_r = \frac{\text{inertial force}}{\text{gravitational force}} = \frac{\rho R^2 V^2/g_c}{\rho R^3 a/g_c} = \frac{V^2}{aR} \qquad (2)$$

Characteristics of Liquid Oscillations

Evaluation of sloshing data from the S-IV stage of the Saturn I vehicles (Reference 1) indicates that during powered flight the LH_2 wave motion was essentially of the fundamental antisymmetric mode with several higher harmonics. The measured frequency of the fundamental mode was in good agreement with the theoretical fundamental frequency. Analyses indicated that the LH_2 sloshing during powered flight of the S-IVB stage was also expected to be predominately of the fundamental mode. Therefore, for purposes of analysis and specification of experiment conditions, only the fundamental mode of antisymmetric sloshing was considered. Figure 1 illustrates the geometry of the problem for a flat bottom cylindrical container.

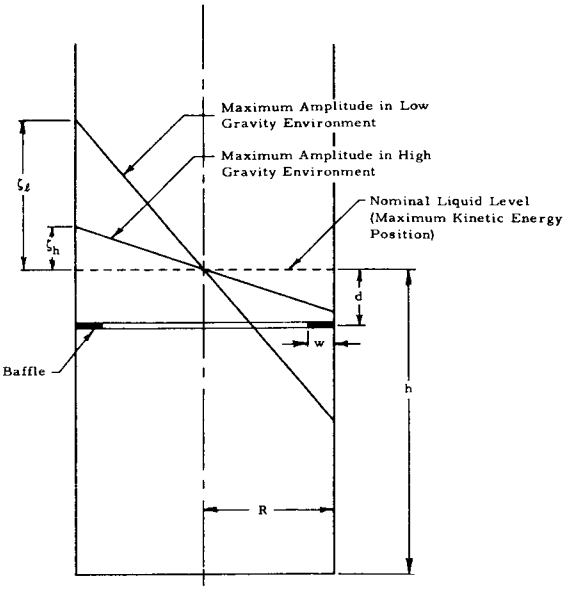

FIG. 1. Geometry for Liquid Oscillations in a Flat Bottom Cylindrical Container

If an inviscid, incompressible liquid is oscillating in a cylindrical container in a high gravity environment, the total energy of the wave motion can be expressed as a function of the sloshing mass, the sloshing frequency, and the maximum liquid amplitude at the container wall.

$$E = 0.21\, m_s\, \omega_h^2\, \zeta_h^2/g_c = 0.21\, m_s\, V_h^2/g_c \tag{3}$$

where the sloshing mass is given as,

$$m_s = 1.43R^3\, \rho\, \tanh\,(1.841\, h/R) \tag{4}$$

The portion of the total energy that is in the potential energy state is

$$P.\ E. = E \sin \phi \tag{5}$$

Satterlee and Reynolds (Reference 2) studied the motions of a liquid in a vertical cylindrical tube under the combined influence of gravitational and capillary forces and obtained data that are in substantial agreement with their theoretical predictions. Based upon a linearized inviscid incompressible analysis, they found that the fundamental frequency can be described by the equation:

$$\omega = \left\{\frac{\beta}{R^3}\, [\tanh\,(1.841\, h/R)]\ \ [6.255 + 1.841\, B_o - 4.755 \cos\theta]\right\}^{\frac{1}{2}} \tag{6}$$

When the capillary forces are essentially negligible relative to the gravitational forces, that is $B_o \gg 1.0$, equation (6) reduces to,

$$\omega = \left\{[\tanh\,(1.841\, h/R)]\ [(1.841\, a/R)]\right\}^{\frac{1}{2}} \tag{7}$$

If a liquid column is oscillating with maximum amplitude, ζ_h, and the applied acceleration is suddenly reduced, the maximum amplitude of the oscillation in the reduced gravity environment, ζ_ℓ, can be estimated from the total energy equation (3) by equating maximum kinetic energy under the high gravity condition to maximum potential energy based on the reduced gravity condition to give,

$$\zeta_\ell / R \approx 0.74 \left(\frac{V_h^2}{a_\ell R}\right)^{\frac{1}{2}} \tag{8}$$

Equation (8) illustrates that the maximum amplification is directly proportional to the liquid velocity before the change in acceleration and inversely proportional to the square root of the final or reduced acceleration. The term (V^2/aR) is recognized as the Froude number. Since under significantly reduced gravitational forces the liquid-vapor interface becomes highly curved, it would be suspected that equation (8) is not an accurate numerical representation of the maximum liquid amplitude in the low gravity environment. It does, however, indicate that the Froude number is the applicable scaling parameter.

The maximum liquid amplitude can also be expressed in terms of an amplification factor, which is simply a ratio of the maximum amplitudes prior to and following the acceleration decrease. That is,

$$\zeta_\ell / \zeta_h = \left[\sin^2 \phi + (a_h/a_\ell) \cos^2 \phi\right]^{\frac{1}{2}} \tag{9}$$

where ϕ is the wave phase angle at the time of the decrease in acceleration. In the special cases where $\phi = 0°$ and $180°$ (flat liquid interface), equation (8) will yield a relation identical to equation (9).

Previous Damping Investigations

If there is no energy input to a system that is oscillating in one of its natural modes, the amplitude of successive oscillations decreases as a result of energy dissipation. The decreasing amplitude can be described by the logarithmic decrement.

$$\delta = \ln \frac{\text{maximum amplitude of any cycle}}{\text{maximum amplitude one cycle later}} = \frac{1}{n} \ln \left(\frac{\zeta_i}{\zeta_n}\right) \tag{10}$$

where ζ_i is the amplitude of the initial cycle and ζ_n is the amplitude n cycles later.

A number of experimental investigations have been conducted under standard gravitational conditions to determine the characteristics of viscous damping of the fundamental antisymmetric mode of oscillation in cylindrical containers as a function of liquid depth, liquid amplitude, kinematic viscosity, and tank size. The experimental investigations produced similar, but not identical, empirical relationships for calculating the logarithmic decrement. Stephens (Reference 3) expressed his results in the form,

$$\delta = 5.23\,(\nu^{\frac{1}{2}} R^{-\frac{3}{4}} a^{-\frac{1}{4}})\left\{\left[1 + 2\left(1 - \frac{h}{R}\right)\operatorname{csch}\left(3.68\,\frac{h}{R}\right)\right]\right.$$

$$\left.\left[\tanh^{-\frac{1}{4}}\left(1.84\,\frac{h}{R}\right)\right]\right\} \qquad (11)$$

The quantity $(\nu^{\frac{1}{2}} R^{-\frac{3}{4}} a^{-\frac{1}{4}})$, commonly called the "damping parameter," includes the kinematic viscosity, acceleration, and tank size as variables. The quantity in brackets describes the effect of the liquid depth on damping. This term becomes a dominant factor as the filling depth ratio, h/R, is decreased below 1.0. For the deep tank problem (h/R > 1.0) equation (11) reduces to,

$$\delta = 5.23\,(\nu^{\frac{1}{2}} R^{-\frac{3}{4}} a^{-\frac{1}{4}}) \qquad (12)$$

Reference 4 summarizes the findings of the Russian investigator, G. N. Mikishev, whose results were obtained in the form,

$$\delta = 4.98\,(\nu^{\frac{1}{2}} R^{-\frac{3}{4}} a^{-\frac{1}{4}})\left\{1 + \frac{0.318}{\sinh\,(1.84\,h/R)}\left[\frac{1 - h/R}{\cosh\,(1.84\,h/R)} + 1\right]\right\} \qquad (13)$$

Both Stephens and Mikishev concluded that the damping was not affected by the liquid amplitude at the wall for amplitudes up to 0.1 R. Applicability of the equations for amplitudes greater than 0.1 R is not known.

Mikishev specifically investigated the effect of surface tension on damping by employing two cylindrical tank diameters (20 cm and 51.8 cm) and test liquids having different surface tensions but identical kinematic viscosity, (Reference 4, page 110). Results of these experiments showed that the surface tension has an increasingly significant effect on damping as the Bond number is reduced. Equations (11) through (13) do not account for the effects of surface tension and are, therefore, limited to large Bond number applications.

More recently, an investigation of damping under conditions of zero Bond number has been performed by Salzman (Reference 5). Salzman shows that the logarithmic decrement for a deep tank in a zero gravity environment is given by either,

$$\delta = 21.6\left(\frac{\nu^2}{\beta R}\right)^{\frac{1}{4}} \qquad (14)$$

or,

$$\delta = 28.1 \left(\frac{\nu}{\omega R^2}\right)^{\frac{1}{2}} \tag{15}$$

For large Bond numbers the quantity $(\nu/\omega R^2)^{\frac{1}{2}}$ is identical to the more commonly recognized damping parameter given in equations (11) through (13). The results of Stephens (equation (12)) expressed in the form of equation (15) are,

$$\delta = 6.1 \left(\frac{\nu}{\omega R^2}\right)^{\frac{1}{2}} \tag{16}$$

Neither equation (15) nor equation (16) appears adequate for predicting damping in the Bond number range of interest during most orbital operations ($B_o \approx 20\text{-}100$), and additional investigation is required to define the variation of the coefficient of the damping parameter with Bond number.

S-IVB-203 LH_2 Sloshing Conditions

One of the primary study objectives was to evaluate the liquid behavior at the conditions anticipated to exist in the S-IVB-203 LH_2 tank at orbital insertion. It is, therefore, of interest to review these specific conditions and the S-IVB-203 geometry.

The Dynamics Analysis Branch of the MSFC Aero-Astrodynamics Laboratory(R-AERO-DD)made an evaluation of the sloshing characteristics of liquid hydrogen in the S-IVB-203 stage during ascent flight. Values pertinent to the problem of liquid motion following orbital insertion, that is after J-2 engine cutoff, are listed in the following table.

TABLE I

S-IVB-203 STAGE LIQUID HYDROGEN SLOSHING PARAMETERS

Tank radius, R	130 inches
Filling height, h/R	0.87
Acceleration prior to J-2 cutoff, $(a/g_o)_h$	3.41
Acceleration following J-2 cutoff, $(a/g_o)_\ell$	5×10^{-4}
Sloshing frequency at J-2 cutoff, f_h	0.70 cps
Maximum amplitude at wall without baffle, ζ_h	5 inches
Maximum velocity at wall without baffle, V_h	1.83 ft/sec
Maximum amplitude at wall with baffle	0.27 inches
Maximum velocity at wall with baffle	0.1 ft/sec

Based upon the values given in Table I, the maximum energy sloshing conditions in the S-IVB-203 LH_2 tank at orbital insertion without baffles correspond to a Froude number of 19.3. From equation (8), a Froude number of this magnitude represents an approximate maximum liquid amplitude following orbital insertion of 3.26 tank radii or about 35 feet with respect to the liquid surface before engine cutoff. Such an amplitude would be in excess of the physical dimensions of the S-IVB-203. The maximum LH_2 energy conditions were considered intolerable from the standpoint of vehicle stability and vent system reliability. Examination of equation (8) shows that the liquid amplification can be minimized by one or a combination of the following methods:

1. Decrease the initial liquid velocity. This may be accomplished by:

   a. Terminating the thrust when the slosh wave is in the minimum kinetic energy position ($\phi = 90°, 270°$)

   b. Decreasing the maximum possible velocity with slosh suppression devices

2. Install deflectors to redirect the flow to the bottom of the tank.

3. Increase the final acceleration level with auxiliary thrusters.

The ideal solution is to terminate the thrust when the wave is in its minimum kinetic energy position, since this theoretically produces no amplification of motion. In the practical case, however, the problems involved in sensing the instantaneous wave position and initiating the engine cutoff signal at a time when the vehicle velocity is also within acceptable limits make this solution unfeasible.

Slosh baffles were evaluated by R-AERO-DD to determine the extent of damping that could be expected on the S-IVB-203 stage using various baffle configurations. The amplitude and velocity given by Table I are for one 20-inch ring baffle placed at the approximate location of the liquid level at J-2 engine cutoff. It was anticipated that the 20-inch ring baffle would reduce the liquid amplitude following cutoff to a maximum of $\zeta_\ell / R = 0.178$ or about 1.90 ft. To achieve the same effect by means of auxiliary propulsion, at least 0.167 g's, or in the case of the AS-203 vehicle, a minimum thrust level of 10,000 lb_f would be required. Of these two alternatives, the ring baffle imposes a much smaller weight penalty, is passive, and can also be used to suppress sloshing during orbital coast. Therefore, a 20-inch ring baffle was installed in the S-IVB-203 LH_2 tank as a propellant control device. As an additional

precaution, a deflector was mounted approximately 100 inches (as measured at the wall attachment point) above the baffle. Figure 2 illustrates the S-IVB-203 fuel tank configuration with the baffle and deflector installed.

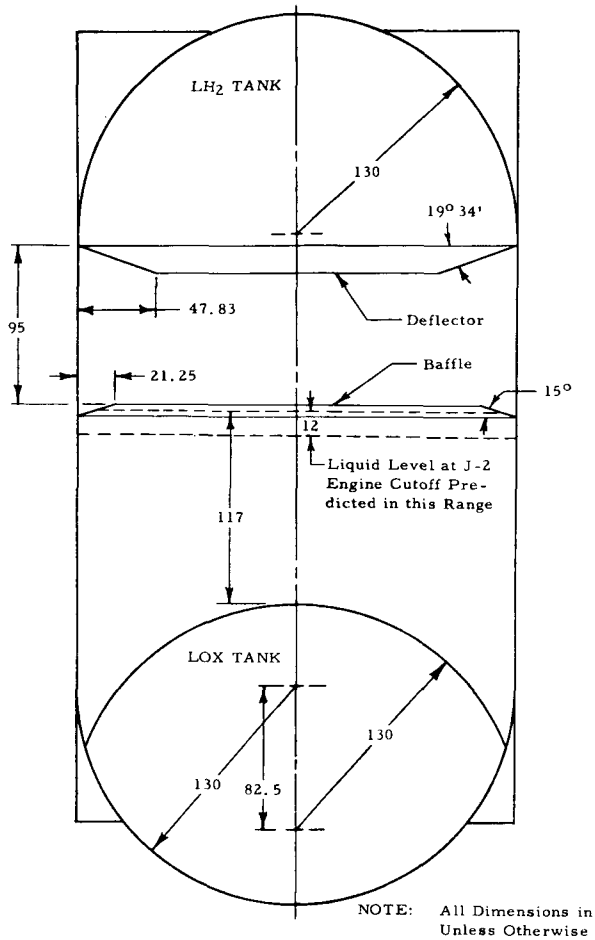

FIG. 2. S-IVB-203 Propellant Tank Geometry

Simulation of S-IVB-203 Conditions

To simulate prototype conditions in the MSFC drop tower, Froude numbers of at least 19.3 (without baffles) were required. The basic drop tower procedure consisted of establishing a first mode slosh wave in the model container and, then, releasing the test package into a low gravity environment. Therefore, assuming maximum energy conditions, the normal gravity liquid amplitude necessary to produce a given Froude number can be expressed as,

$$\zeta_h/R = \left[\frac{F_r(a/g_o)_\ell \; g_o}{\omega_h^2 R}\right]^{\frac{1}{2}} \tag{17}$$

Equation (7) accurately defines the oscillation frequency of a liquid in containers of a few inches or greater in diameter under standard gravitational conditions. Substituting equation (7) into equation (17), the amplitude becomes,

$$\zeta_h/R = 0.737 \left[\frac{F_r(a/g_o)_\ell}{\tanh\ (1.841\ h/R)\ (a/g_o)_h}\right]^{\frac{1}{2}} \tag{18}$$

Thus, if the Bond number is sufficiently great at the conditions before the reduction in acceleration, simulation of a given Froude number is independent of the test container dimensions or physical properties of the test fluid. Equation (18) is plotted in Figure 3.

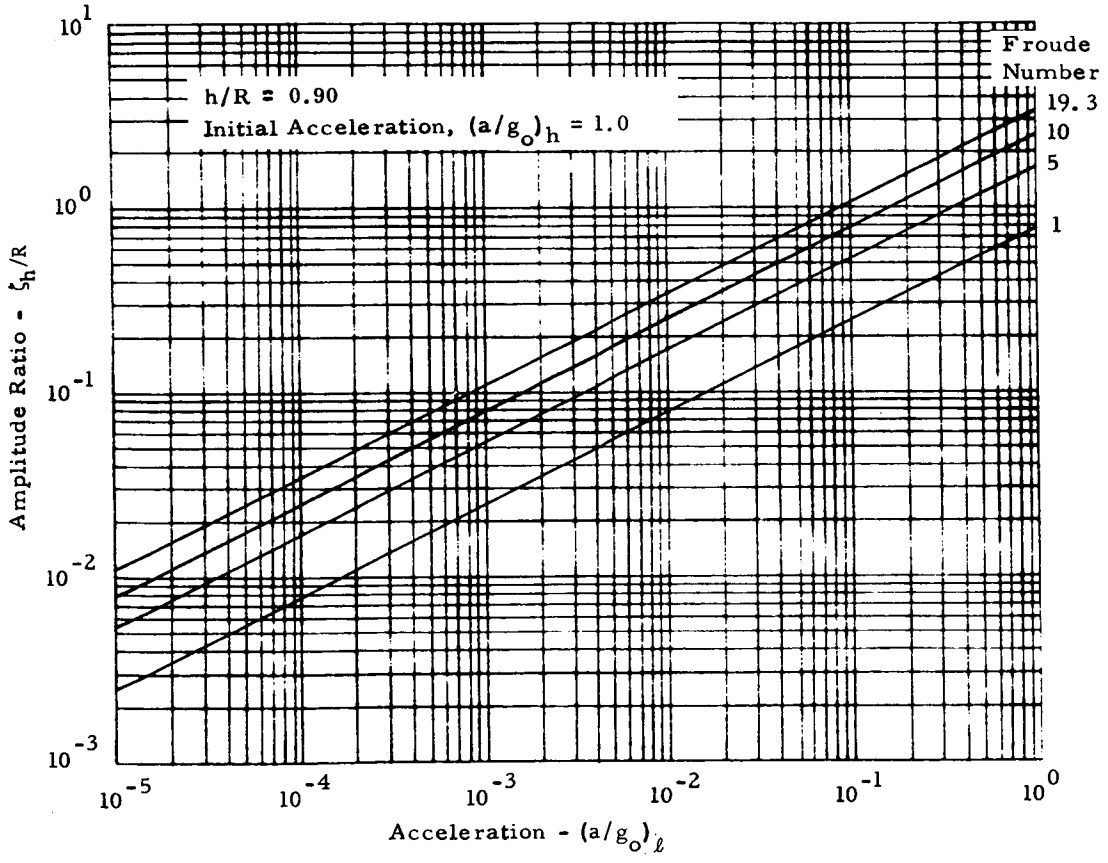

FIG. 3. Test Conditions Required to Produce Various Froude Numbers

Figure 3 illustrates that at the reduced acceleration levels for which the drop tower was initially checked out ($a/g_o \approx 10^{-2}$), liquid amplitude ratios of at least $\zeta_h/R = 0.35$ were required to produce Froude numbers of the magnitude anticipated in the S-IVB-203 fuel tank at orbital insertion without baffles.

APPARATUS AND PROCEDURES

Test Program Outline

The initial tests utilized a six-inch inside diameter Lucite scale model S-IVB liquid hydrogen tank. Prior to the AS-203 flight, the primary objectives of the program were to study the comparative liquid behavior with and without the baffle and deflector in the tank and to obtain an indication of the expected liquid behavior at orbital insertion. After data pertinent to the AS-203 flight were obtained, the LOX-LH_2 common bulkhead was replaced with a flat base, and additional tests were performed to provide data over a wider range of conditions for general application to the design of liquid storage systems. The experimental program consisted of the following general test series.

1. Scale model S-IVB tank with no baffle or deflector and a liquid height of $h/R = 0.9$. Liquid amplitudes before the drop were varied from $\zeta_h/R = 0.35$ to 0.85 to simulate AS-203 energy conditions without the baffle. Reduced accelerations ranged from 0.01 to 0.026 g_o.

2. Scale model S-IVB tank with geometrically-scaled baffle and deflector. Reduced accelerations ranged from 0.005 to 0.01 g_o.

3. Six-inch inside diameter flat bottom circular cylinder with no baffle and an $h/R = 1.3$. Liquid amplitudes before the drop were of low amplitude ($\zeta_h/R = 0.08 - 0.2$) to produce more nearly ideal linear motion. Reduced accelerations ranged from 0.01 to 0.04 g_o.

Test Facility

The test program was conducted in the MSFC drop tower facility, which is located in the Saturn V Dynamic Test Tower. The experiment package containing the scale model tank and associated equipment was placed inside a protective drag shield, suspended from the top of the Dynamic Test Tower, and dropped into a 40-foot tall pneumatic (air) tube that decelerated the drag shield and experiment package. During the drop, the experiment package was free floating within the drag shield.

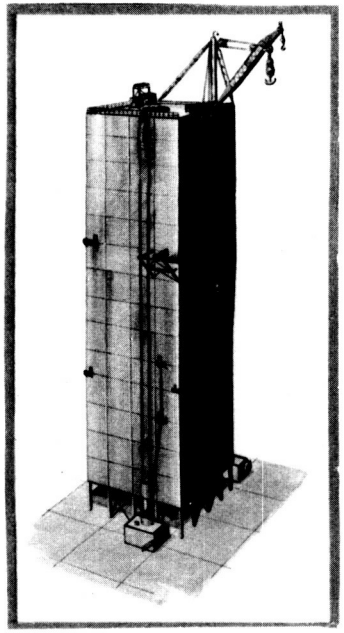

SATURN V DYNAMIC
TEST STAND

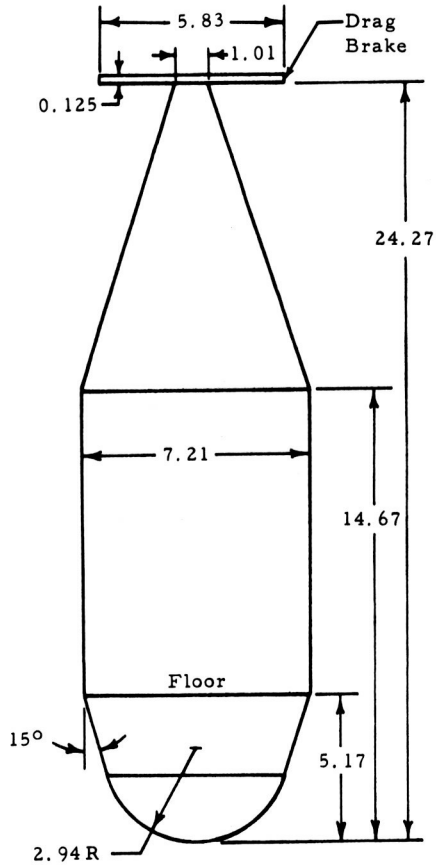

DRAG SHIELD

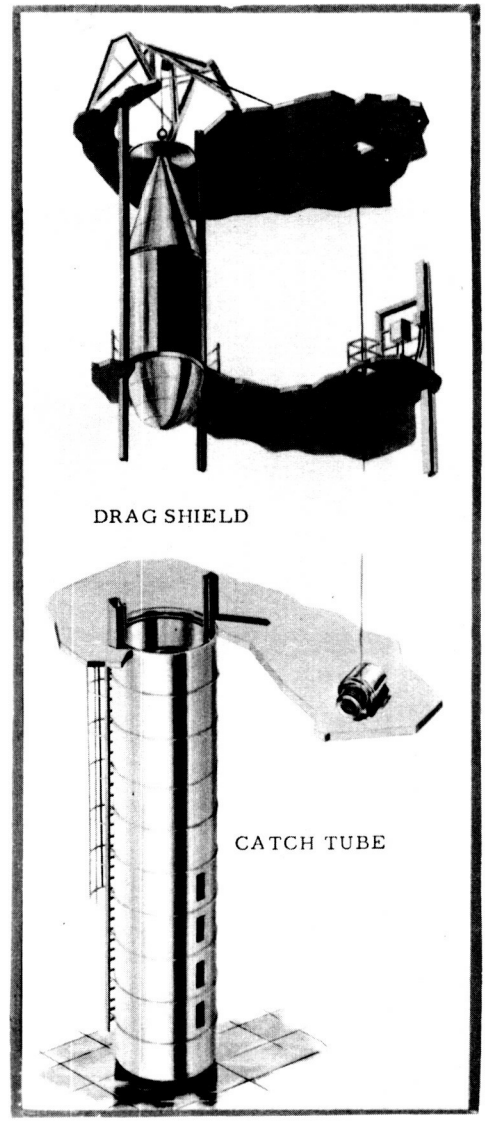

FACILITY CAPABILITIES

PAYLOAD	450 lbs.
LOW GRAVITY TEST RANGE	
MINIMUM	10^{-5} g_o
MAXIMUM	4×10^{-2} g_o
DROP TIME	4.3 sec.
TOTAL DROP WEIGHT	4000 lbs.
MAXIMUM TEST PACKAGE	3' dia. x 3' high
DECELERATION	less than 25 g's

FIG. 4. Marshall Space Flight Center Low Gravity Test Facility

The drop distance between the bottom of the drag shield (when suspended at the top of the tower) and the top of the pneumatic tube is approximately 294 feet, permitting low gravity test durations of up to 4.3 seconds. Because of the drop height and the small diameter differential between the drag shield O. D. and the pneumatic tube I. D. (3 inches), the drag shield is guided during the drop by rails. Figure 4 is a composite showing various physical characteristics and capabilities of the facility. References 6 and 7 provide additional details concerning the facility and its operation.

Experiment Package

The experiment package consisted of a 3 x 3 x 1.5 foot welded angle aluminum frame with a plywood floor to which was mounted the necessary test equipment (Figure 5). The model tank was clamped to the sliding table of a solenoid spring-operated mechanism (Figure 6) and enclosed within a light box, which provided proper light distribution on the test specimen for high-speed photography. The mechanism was used to establish the initial slosh wave in the liquid. When the solenoid is energized, the spring forces the tank assembly along the slide rod and against the opposite side of the base frame. The motion of the test container and the impact against the base frame results in the formation of a slosh wave in the liquid. The mechanism was constructed so that waves of varying initial maximum amplitude could be established in the test fluid by altering the spring constant, the spring tension, the travel of the sliding table, or any combination of these variables.

The electrical power for the experiment package was supplied by rechargeable nickel-cadmium batteries carried on the package. Data (except photographs) were originally retrieved from the package through a trailing cable between the experiment package and the drag shield. The data cable was the only physical connection between the experiment package and the drag shield during dropping. To eliminate this trailing cable, a telemetry data retrieval system was designed and incorporated after approximately 50 percent of the test program was completed.

A nitrogen cold gas thruster located in the center of the package and exhausting downward through an opening in the center of the floor was used to apply a predetermined acceleration to the test fluid during drop. Gas was supplied to the thruster from a 3000 psia storage bottle mounted on the experiment package. The thruster nozzle was calibrated in the form of plenum pressure versus thrust by a precision force-balance technique. By adjusting a pressure regulator on the package,

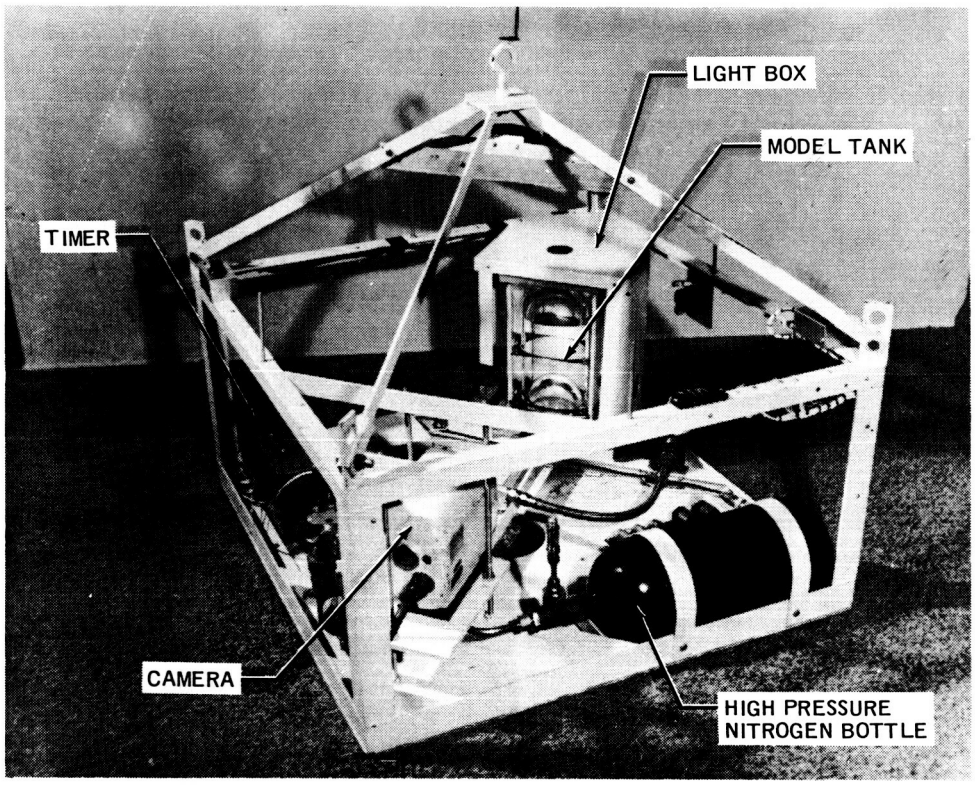

FIG. 5. Drop Tower Experiment Package

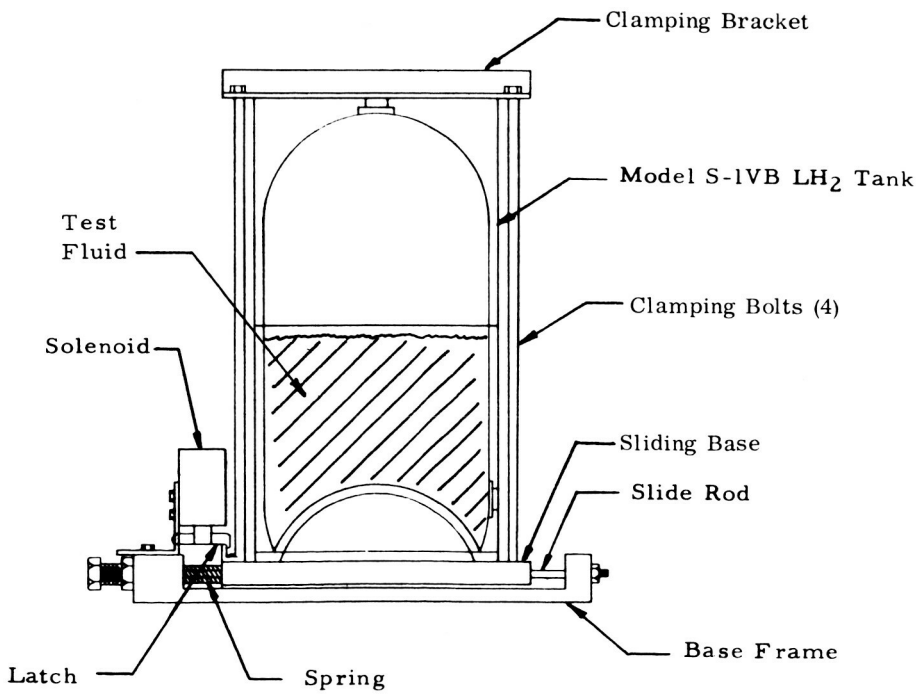

FIG. 6. Sketch of Impulse Mechanism with Model Tank Installed

the thruster plenum pressure could be changed to vary the acceleration on the package from one drop to another.

Test Liquid

The test fluid used in all cases was petroleum ether. Petroleum ether was selected because it has a kinematic surface tension that is nearly the same as hydrogen, has a static contact angle of zero degrees with Lucite, and is chemically compatible with Lucite. To ensure proper wetting, careful cleaning procedures were adopted, and contamination of the solid surfaces and the liquid was avoided. The density, surface tension, and viscosity of petroleum ether were each measured at three different temperatures within the range of interest. The test fluid temperature was measured before each drop so that fluid properties characteristic of each test could be evaluated. The following table lists values of these properties.

TABLE II

PROPERTIES OF PETROLEUM ETHER

Temperature		Density		Temperature		Surface Tension		Temperature		Viscosity	
^{o}C	^{o}F	gm/cm^3	lb_m/ft^3	^{o}C	^{o}F	dyne/cm	lb_f/ft	^{o}C	^{o}F	centistokes	$lb_m/ft\ sec$
26.7	80.06	0.6185	38.61	21	69.8	14.9	1.021×10^{-3}	21	69.8	0.39	1.672×10^{-4}
21.0	69.8	0.6382	39.84	10	50.0	16.2	1.11×10^{-3}	10	50.0	0.43	1.86×10^{-4}
15.6	60.08	0.6433	40.16	-4	24.8	17.3	1.185×10^{-3}	-4	24.8	0.47	2.04×10^{-4}

Operating Procedure

After the experiment package was assembled, the camera loaded with film, the thruster nozzle centered, the high pressure nitrogen storage bottle charged with gas, and the mechanism placed in the drop position, the package was balanced about the vertical axis of the thrust nozzle by adding weights where required. The balancing was performed on a Bytrex Center-of-Gravity Locator, which is a strain-gauge balance table capable of locating the package center of gravity within ± 0.003 inches. When all balancing was completed, the package was placed in the drag shield, and the drag shield was suspended in its predrop position in the working area at the 336-foot level of the Dynamic Test Tower.

The camera, lights, and thruster were actuated two seconds before the drop to allow the thruster plenum pressure to become fully stabilized

and the camera to attain full speed. An infinitely variable 0-10 second timer on the package was preset to actuate the impulse mechanism at any desired time between camera-on and drop. The camera, lights, and thruster operation were terminated by onboard circuitry approximately nine seconds after initiation. The entire test sequence was executed automatically.

Data Reduction

To visually and numerically evaluate the liquid behavior, films were taken of the test container and liquid at a speed of about 400 frames/sec with a Milliken camera. Numerical data pertinent to the liquid motion were obtained by reading, with a Teleredex machine, the liquid amplitude as a function of time (in a plane perpendicular to the field of view of the camera) from the film. Ordinarily, the amplitude was read every fourth frame, or at approximately 0.01-second intervals, providing about 40-45 data points per cycle of liquid motion under one-g conditions and 200-400 points per cycle under the reduced gravity conditions.

Film Calibration - To correct for the visual distortion due to the tank wall and the test fluid, a calibration grid of horizontal and vertical ruled lines on a Plexiglass sheet was placed in the test tank and aligned on a plane passing through the center line of the tank. The tank was then filled with petroleum ether and photographed under conditions identical to those used on the experiment package, that is, with the same camera, lens, and spacing between the lens and test tank. From the calibration film, a table was compiled in the form of apparent horizontal and vertical distance as a function of known ruled distance. This table was input to a data reduction computer program and used to correct "as read" dimensions to true dimensions before any other operations or calculations were performed with the data.

Experiment Package Acceleration - During each test, the thruster plenum pressure was measured continuously to determine the variation in pressure. The pressure traces indicate that the thrust remained nearly constant during any given drop. The maximum variation observed between the pressure at the beginning of a test and the pressure at the end of the test was about 3.5 percent. Using the average measured pressure, the actual thrust was determined from the nozzle calibration curve. The acceleration level was subsequently calculated from the thrust-mass characteristics of the package.

During the final series of tests in the program, a low-range accelerometer (Model MCA-5 linear accelerometer manufactured by Universal Controls, Incorporated) was installed on the experiment package. The instrument used is a high performance, servo-type, force balance transducer having an output of ± 5 volts DC at ± 0.2 g's. Comparisons of the acceleration indicated by the accelerometer and the acceleration calculated from the package thrust-mass characteristics show that the accelerometer reading was usually higher than the calculated acceleration. The difference between the measured and the calculated acceleration was greatest at the lower acceleration levels. The accelerometer reading was a maximum of about 20-25 percent higher than the calculated acceleration at 0.04 g's but was as much as 100 percent higher than the calculated value at 0.01 g's.

Figure 7 illustrates a typical nominal accelerometer output. Before the drop, the accelerometer output is at full-scale deflection. Following release, a relatively short transient is observed until the accelerometer indicates that a steady-state low gravity condition has been achieved. It is not known whether the initial transient is a result of the instrument response characteristics or an actual gravity transient. It is probably a combination of the two, but the individual effects cannot be separated. The exact nature of the transient profile varied somewhat from one test to another, but the accelerometer indicated steady-state conditions from 0.1 to 0.3 seconds after first package motion. In the example illustrated by Figure 7, the calculated acceleration was 0.0404 g's, while the accelerometer indicated 0.05 g's.

Although the accelerometer characteristics discussed in the previous paragraphs were typical, there were several instances in which the nozzle thrust was varied to increase or decrease the acceleration on the package; yet, the accelerometer indicated the opposite effect. In all cases the wave period measured in the low gravity environment supported the calculated acceleration both in trend (period increases with decreasing acceleration) and in absolute numerical value (equation (6)). The reasons for the discrepancies in the accelerometer output could not be resolved. Therefore, the experimental data were evaluated on the basis of the calculated acceleration levels.

Determination of Release Time - Coded timing marks were displayed along the edge of the film to relate the film to the physical events occurring during the test sequence. The time of release of the experiment package and drag shield was indicated by a breakwire signal. When viewing the films, it appeared that the liquid was experiencing a reduced gravity environment before the breakwire signal. After installation of

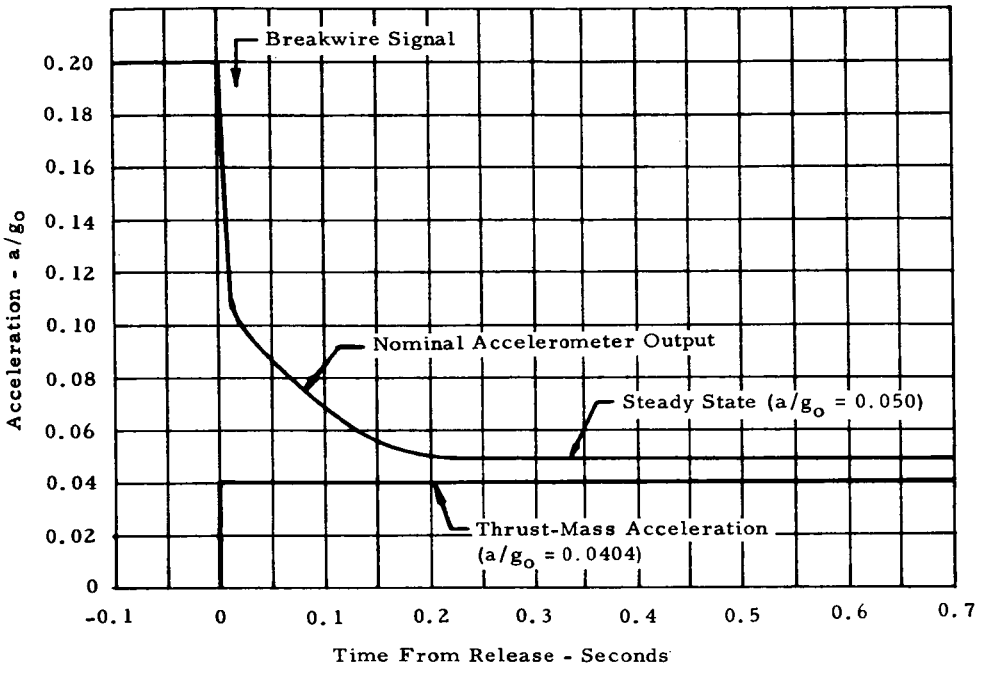

FIG. 7. Typical Low Gravity Accelerometer Output and Comparison with Calculated Acceleration

the accelerometer on the experiment package, this fact was validated. The accelerometer consistently indicated motion of the experiment package from 0.01 to 0.03 seconds before the breakwire signal. In the test illustrated by Figure 7, for example, the breakwire signal occurred 0.02 seconds after the accelerometer first indicated package motion. This time lag was subsequently attributed to varying degrees of stretching of the wire between the time of release of the drag shield and the actual breaking of the wire. The zero time on the films was, thereafter, adjusted for the time lag.

Determination of Liquid Velocity - The liquid velocity at the instant of release into the low gravity environment was one of the primary parameters of interest in the tests. To obtain this data, a least squares second order polynomial curve fit was applied to the amplitude data using an arbitrary number of data points. By differentiating the resulting polynomial, the liquid velocity at the time corresponding to the midpoint of the particular data group was obtained. This procedure will be clarified by referring to Figure 8.

If a five-point (must be an odd number) curve fit is chosen, a polynomial is fit to the first five data points as illustrated by Figure 8. The polynominal is then differentiated and evaluated at the time correspond-

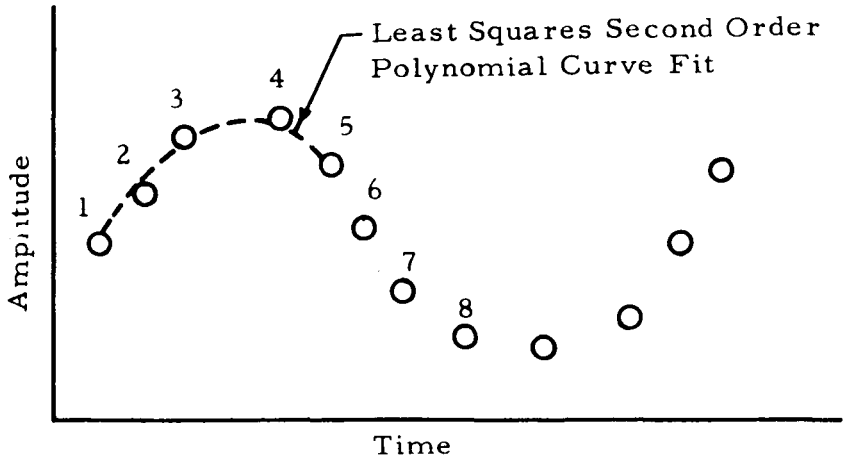

FIG. 8. Illustration of Amplitude Data Curve Fitting Procedure

ing to data point 3 to give the velocity at point 3. This procedure is repeated using points 2 through 6, inclusive, to obtain the velocity at point 4, and so forth. By this method, a three-point fit describes the instantaneous velocity based upon the "as read" amplitude data. Use of a greater number of points in the curve fit produces smoothing of the "as read" data.

The test films indicated that during the oscillation, which was established before the drop, the liquid immediately adjacent to the wall sometimes appeared to become "stuck" to the wall, although liquid a short distance away from the wall was moving. The "stuck" condition occurred when the wave reached its minimum or maximum amplitude (zero velocity) and changed direction. If the release of the experiment package occurred while the liquid was stuck, or shortly after the breakaway from the wall, the stuck condition might significantly affect the linearity of the velocity profile with the maximum instantaneous velocity occurring at some distance from the wall. Consequently, the velocity profile across the liquid surface was determined for each test.

To determine the velocity profile across the liquid surface, the amplitude history of the surface was measured at 0.15 inch increments up to about one inch from the wall over the time period from 0.3 seconds before the drop until 0.3 seconds after the drop. The transient velocity of the surface at each radial station was then computed from a curve fit in the manner described previously. The results of the foregoing procedure definitely established that the maximum liquid velocity at the time of release was not always at the tank wall. This is illustrated by

Figure 9, which shows the velocity profiles across the liquid surface at various times before and at the time of drop during test 2F-28. All values in Figure 9 are based on a five-point curve fit.

The effect of the number of points chosen for the curve fit on the magnitude of the reduced numerical data was also investigated. The velocity profiles were evaluated on the basis of 5, 11, and 19-point curve fits to determine the effect of the curve fit on the computed numerical value of the velocity. Several comparisons were also made, which included a three-point fit, and it was found that the three- and five-point fits produced nearly identical velocities. Once this was established, the three-point fit was omitted from subsequent evaluations. Omission of the three-point fit was based on reasons associated with the operation of the data reduction computer program. Figure 10 shows the effect of the number of points chosen for the curve fit on the velocity profile at breakwire time during test 2F-28. In this particular case, the velocity at the wall computed from the five-point fit is about twice as great as the velocity obtained from a 19-point fit.

As suggested by equation (8), the maximum liquid amplitude in the low gravity environment was plotted against the square root of the Froude number where the maximum instantaneous velocity in the liquid at release was used to compute the Froude number. Plots were made using five- and 19-point fits to determine the velocity. Whereas the data based on the 19-point velocities were so scattered as to be completely meaningless, the data based on the five-point velocities demonstrated the expected trend (maximum amplitude decreases with decreasing Froude number) with significantly less scattering of the data. It was concluded that the curve fit, and not the velocity profile, was the significant factor in determining the most realistic value of instantaneous velocity.

RESULTS AND DISCUSSION

Maximum Liquid Amplitude Without Baffles

General Liquid Behavior - The general nature of the liquid behavior that was observed in the tests without the baffle and deflector may be divided into two types. The first type of motion occurs when the energy conditions are insufficient to result in the movement of liquid to the top of the tank. As the amplitude of the wave at the tank sidewall where the velocity is positive (toward forward dome) at the time of

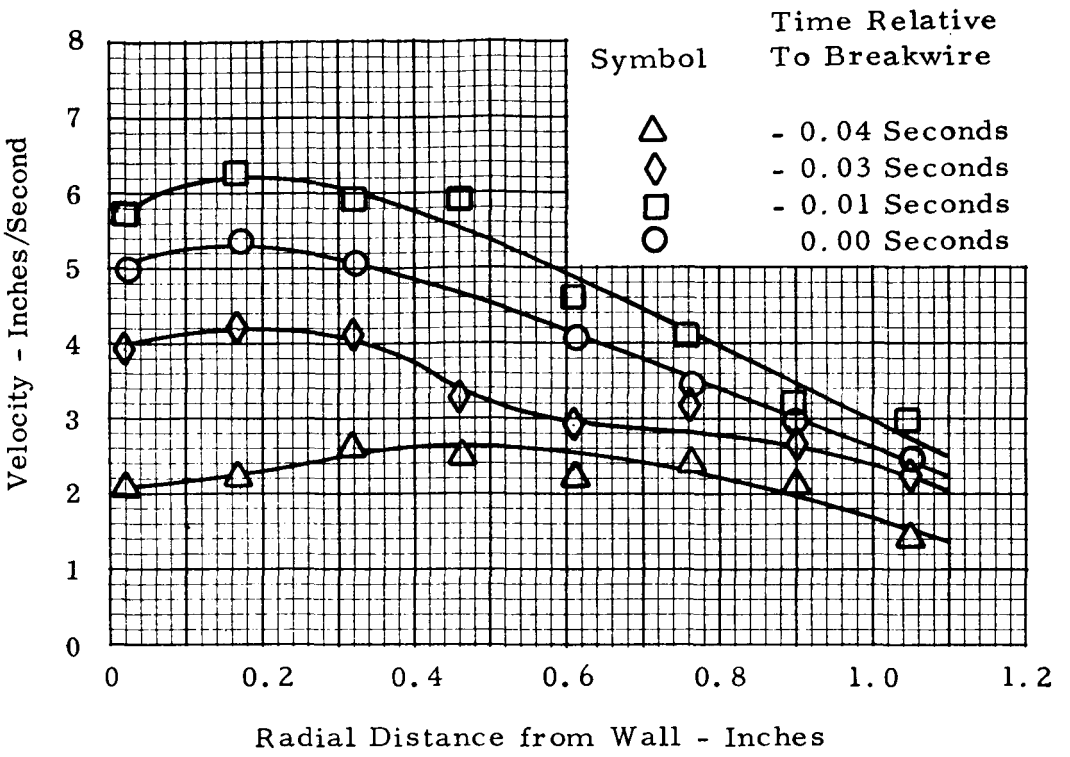

FIG. 9. Liquid Velocity Profiles Based on a Five Data Point Curve Fit

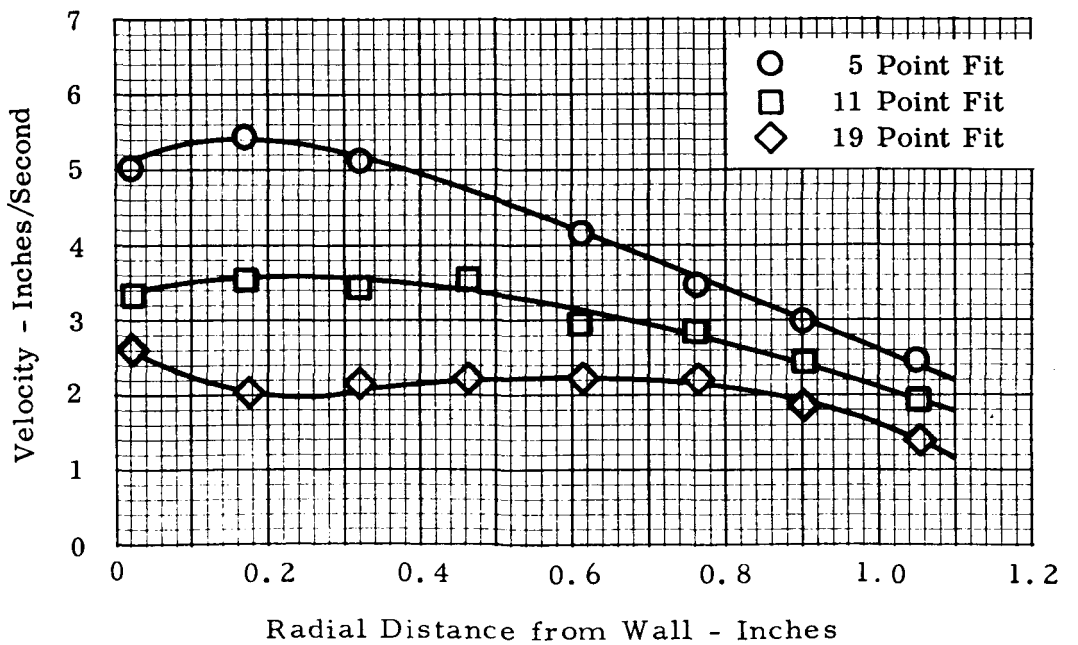

FIG. 10. Effect of the Curve Fit on Calculated Velocities at Breakwire Time

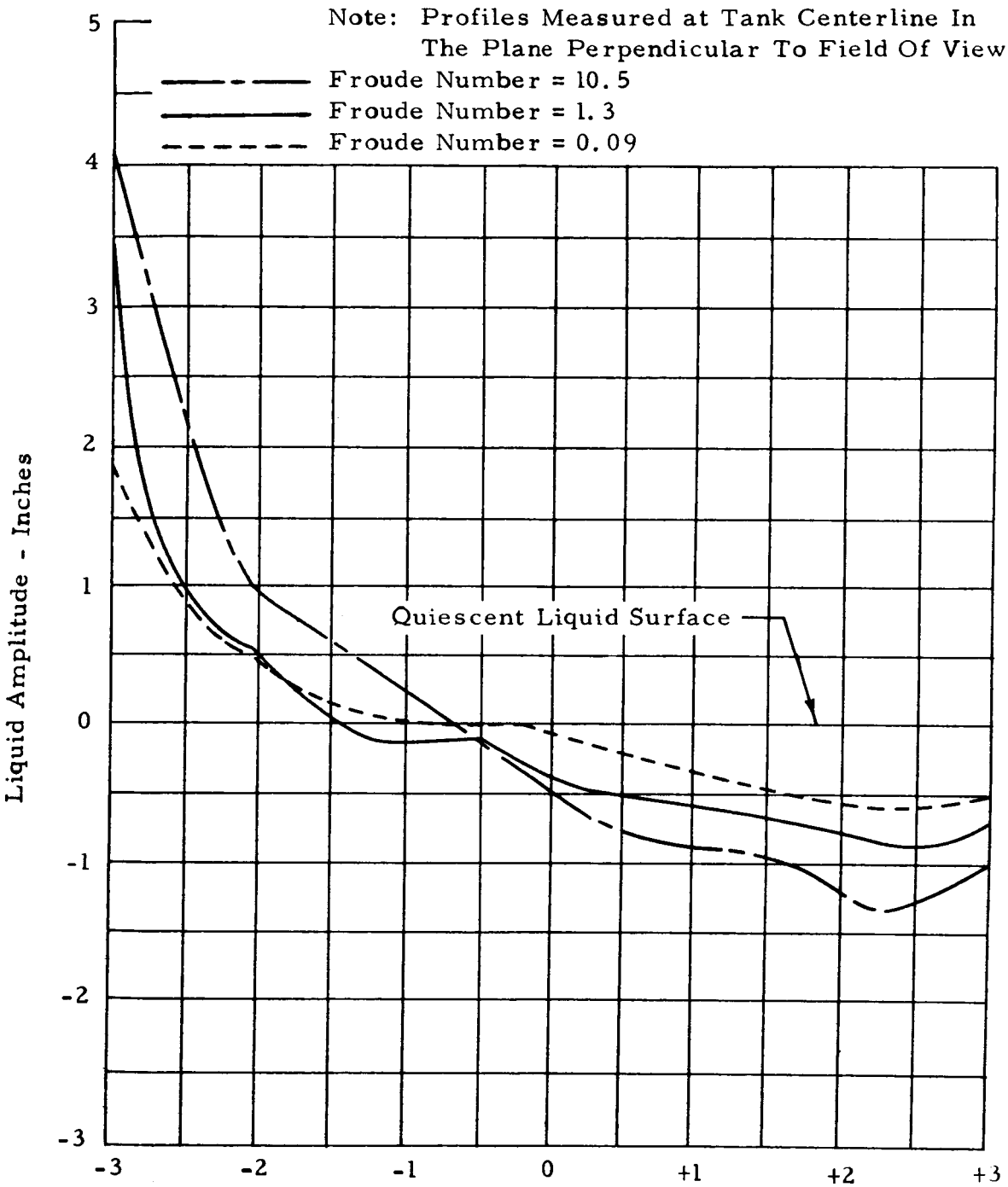

FIG. 11. Liquid-Vapor Interface Profiles at Maximum Amplitude for Various Froude Numbers

release increases with time, the liquid-vapor interface becomes highly curved, but generally remains well-defined. Figure 11 illustrates liquid-vapor interface profiles when the liquid is at its maximum amplitude in the low gravity environment for Froude numbers of 0.09, 1.3, and 10.5.

The second type of motion results when the energy conditions are sufficient to cause movement of the liquid to the top of the tank. In this case, the liquid motion is governed by the particular container geometry. In the model S-IVB tanks, for example, the curvature of the forward dome redirected the flow across the dome and down the opposite sidewall. The initial tests in the experimental program were designed to produce Froude numbers in the approximate range of the predicted S-IVB-203 LH_2 conditions (19.3) without the baffle. Froude numbers as high as 22 were achieved. It was found that the liquid amplitude reached the top of the tank whenever the Froude number was in excess of about 14. These tests did not provide data of numerical value except as applied to the geometry of those specific tests. However, the visual observation of the liquid behavior was informative.

Test 2F-1 affords a good illustration of the general characteristics of the second type of motion. Figure 12 shows selected frames from the film of the test that visually illustrate the liquid configuration at various times. At release, the liquid on the left side of the container moved toward the top of the tank, and as shown by the sequence of photographs, the liquid continued its upward travel until it reached the forward dome. The liquid then followed the contour of the dome, fell down the opposite wall, and re-collected in the bottom of the container. For a short period of time, the liquid appeared to be completely resettled, although some turbulence was visible. However, a second wave containing significantly less mass than the first subsequently rose up the left wall of the tank and reached the top of the dome a second time. The second wave did not completely encircle the dome but, instead, gradually settled back down the left wall. The time interval between the waves corresponded very closely to the natural frequency of the liquid at the reduced gravity level, as determined from the Satterlee-Reynolds equation (equation (6)).

When the liquid fell down the right wall, after its initial pass across the dome, it penetrated the liquid mass that had remained in the bottom

of the tank and entrained a large bubble of ullage gas. The bubble was subsequently transported into the space between the sidewall and the common bulkhead and then slowly gravitated toward the liquid surface (see Figure 12f).

Quantitative Results - The maximum liquid amplitude in the low gravity environment was evaluated in the form of the measured amplitude as a function of the instantaneous energy conditions at drop (as described by the Froude number in equation (8)) and the amplification factor (equation (9)). When considering the results in the form of equation (8), the maximum low gravity amplitude was defined as the difference between the measured maximum amplitude ζ_ℓ, and the instantaneous amplitude at the instant of drop, ζ_i. This amplitude difference is denoted as $\Delta\zeta_\ell$.

Figure 13 shows the measured maximum liquid amplitudes plotted in dimensionless form $\Delta\zeta_\ell/R$, as a function of the square root of the Froude number. Results are shown for tests both with and without the baffle and deflector. In the tests without the baffle and deflector, there was some data scatter, and a single curve representative of all the data could not be defined. However, the maximum amplitude along the upper boundary of the data region varied from $\Delta\zeta_\ell/R = .63$ to $\Delta\zeta_\ell/R = 1.8$ over a Froude number range of 0.028 to 14.6 and is defined by the empirical relation,

$$\Delta\zeta_\ell/R = 0.99\,(Fr)^{[0.018\,\ell n(Fr) + 0.177]} \qquad (19)$$

The numerical data with the baffle in the tank were obtained from tests in which the nominal liquid level was below the baffle position. Figure 13 shows that at any given Froude number the slosh baffle significantly reduced the maximum liquid amplitude compared to the unbaffled amplitude. These results do not fully emphasize the effectiveness of the baffle as a propellant control device. It was shown in Section II. D that the primary value of the baffle is in reducing the liquid kinetic energy (hence Froude number) during the high gravity condition in comparison to the energy that would exist if the baffle were not in the tank.

Within the range of test conditions the maximum liquid amplitude appears to be independent of the Bond number. However, at sufficiently low values of Froude number, a Bond number dependence should become apparent. In the extreme case of an initially quiescent liquid ($F_r = 0$) subjected to a sudden decrease in acceleration, Fung (Reference 8) has shown mathematically that the interface oscillates about its low gravity equilibrium position. This has also been demonstrated experimentally

by Siegert (Reference 9). As the Froude number decreases, the maximum liquid amplitude (as defined in Figure 13) should, therefore, approach, as a minimum value, the wall amplitude of the equilibrium interface configuration corresponding to the prevailing Bond number.

The cause of the data scatter in Figure 13 is probably due to a combination of several factors of which the identification of the release time or zero reference is the most significant. It became apparent early in the program that meaningful amplitude data would be highly dependent upon accurate determination of the zero, or release time. Consequently, great care was exercised to this end. Nevertheless, as illustrated by Figure 9, errors of only a few hundredths of a second in identifying the film frame corresponding to actual release time can result in sizeable errors in initial velocity. Also, it is significant that the data from the tests in which the initial (one-g) sloshing conditions were small in amplitude and more nearly linear in nature, with only one exception, plot along the upper boundary of the data region. This consistency exists because fluid conditions were more uniform from one test to another, and the near linear motion should have permitted more reliable reduction of data from the films. The initial sloshing characteristics in the small amplitude tests were also representative of the type of motion that would occur in a vehicle during powered flight. For these reasons, it is believed that the upper boundary of the data area, as well as being the safe design condition, is actually the most realistic.

The measured and calculated (equation (9)) amplification factors are tabulated in Table III. As shown, the results are inconclusive. The deviations in this case can also be partially attributed to possible errors in determining the exact release time. However, the fact that a reasonably good correlation was obtained in terms of the Froude number, whereas for the same tests nearly random results were obtained in the form of the amplification factor, is explained by the following reasoning. In Figure 13, the measured amplitudes are related to a quantity in which the instantaneous energy conditions were determined from measurements of the liquid surface. On the other hand, the calculated amplification factors in Table III are predicated upon an idealized linear wave in which there is a known relationship between wave phase angle and velocity. Since the actual liquid oscillations were not completely

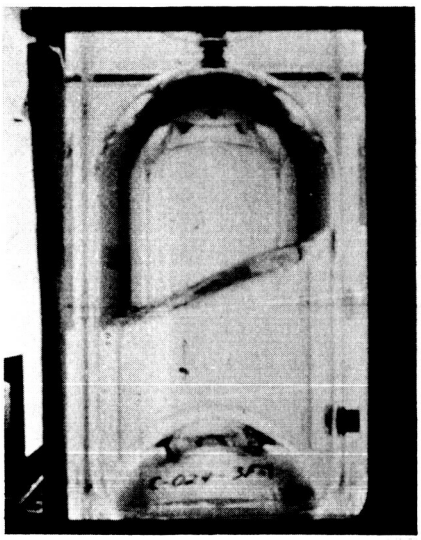

(a) Time = -0.1 seconds (Before Drop) Maximum Amplitude Under Standard Gravitational Conditions

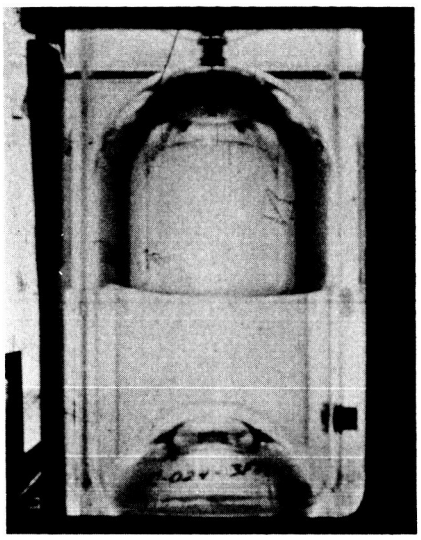

(b) Time = 0.0 seconds (Drop)

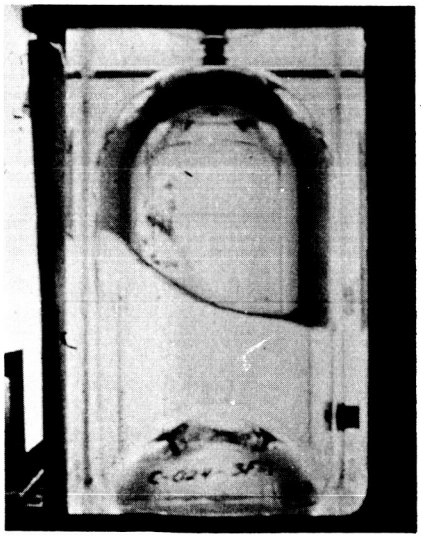

(c) Time = +0.1 seconds (After Drop)

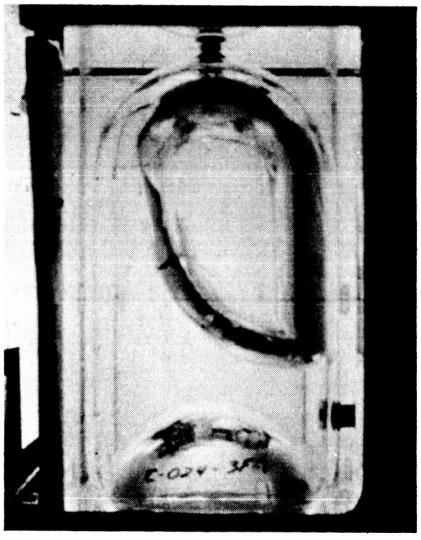

(d) Time = +0.5 seconds. Liquid Reaches Forward Dome of Tank

FIG. 12. Behavior of a Slosh Wave Following a Sudden Reduction in Acceleration, Froude No. = 22

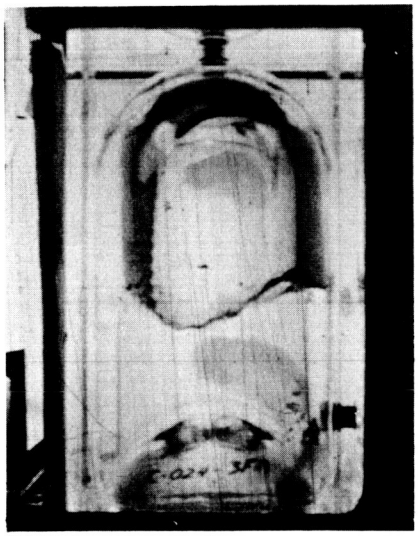

(e) Time = +1.5 seconds. Liquid Begins Re-Collecting in Bottom of Tank

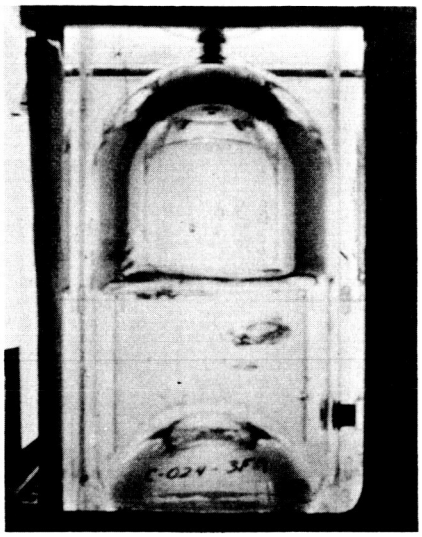

(f) Time = +2.9 seconds. Liquid Appears Settled

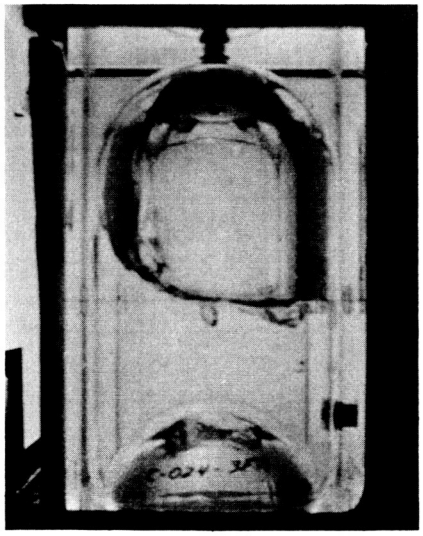

(g) Time = +3.5 seconds. Second Wave Reaches Forward Dome.

FIG. 12. Behavior of a Slosh Wave Following a Sudden Reduction in Acceleration, Froude No. = 22 (Concluded)

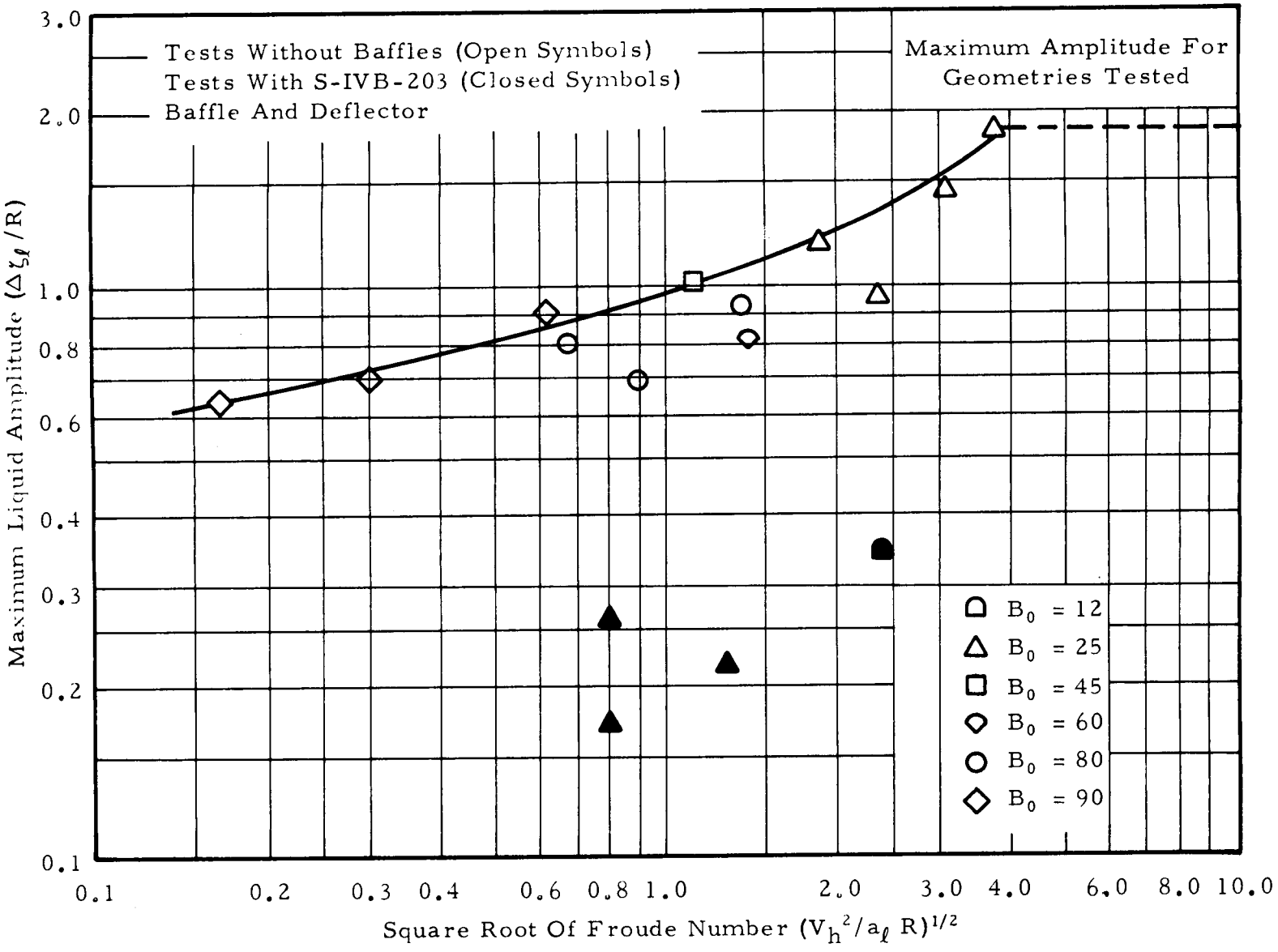

FIG. 13. Maximum Liquid Amplitude Following A Sudden Reduction in Acceleration

linear (see Figure 9) the phase angle was not an accurate representation of the instantaneous velocity.

TABLE III

COMPARISON OF MEASURED AND CALCULATED AMPLIFICATION FACTORS

Test No.	Degrees ϕ	a_h/a_ℓ	Measured			Calculated (Equation 9) ζ_ℓ/ζ_h
			Inches ζ_h	Inches ζ_ℓ	ζ_ℓ/ζ_h	
2F-2	48.5	40.5	1.758	2.775	1.58	4.28
2F-20	119.1	100	0.518	3.391	6.55	4.94
2F-21	31.2	100	0.290	3.050	10.50	8.57
2F-22	142.9	100	0.190	3.890	20.45	8.0
2F-28	9.36	32.3	0.700	1.790	2.56	5.60
2F-30	47.3	33.6	0.391	3.183	8.15	4.0
2F-41	52.6	32.0	0.281	2.608	9.28	3.52
2F-42	47.2	32.0	0.254	1.822	7.17	3.92
2F-46	87.6	26.75	0.310	3.009	9.68	1.023
2F-48	65.7	50.0	0.262	3.263	12.45	3.05
2F-49	27.0	25.64	0.379	1.978	5.21	4.54
2F-50	55.8	25.64	0.397	2.155	5.43	2.96

On the basis of this study it is not possible to derive a conclusive empirical relationship for the liquid amplitude following a reduction in acceleration. However, for unbaffled tanks, equation (19) should provide estimates of sufficient accuracy for most engineering purposes. The amplitudes corresponding to the measured Froude numbers are such that the use of auxiliary devices for reducing the propellant motion would be required in most practical applications.

Tests with Baffles

Eleven tests were conducted with a geometrically-scaled S-IVB-203 baffle and deflector in the model tank. It was originally intended that the nominal liquid level in the S-IVB-203 LH_2 tank be at the baffle position at orbital insertion to derive maximum damping from the baffle immediately before thrust termination. It was estimated, however, that the liquid level could be as much as 12 inches below the baffle at thrust termination due to possible variations in initial propellant loading and flight trajectory. Five tests were performed with the liquid level at the

baffle position, and six tests were conducted with the liquid level a distance of d/R = 0.18 below the baffle. (This corresponds approximately to the minimum predicted S-IVB-203 liquid level at orbital insertion.)

Liquid Level at Baffle Position - In the tests with the liquid level at the baffle position, it was impossible to accurately measure liquid velocities at the wall because of the visual interference of the baffle. Therefore, the results of this particular series of tests are purely qualitative. Pairs of tests were conducted with and without the baffle and deflector installed in the tank. For each pair of tests the initial energy input (mechanism spring constant, spring deflection, and time lag from impulse to drop) and acceleration during drop were, for all practical purposes, identical.

Figure 14 shows selected frames from the films of two tests (2F-19 and 2G-3) that illustrate typical results observed during this series of tests. The Froude number in the test without the baffle was 14.6. The Bond number in both tests was about 24. The energy conditions were such that the maximum amplitude of the liquid in the low gravity environment during test 2F-19 was just equal to the physical upper limits of the tank.

As shown by Figure 14, the maximum liquid amplitude with the baffle was considerably lower than observed in the corresponding test without the baffle. In addition, a thin column or "spike" of liquid was formed near the wall that subsequently flowed upward and away from the tank wall toward the opening in the center of the deflector. The column reached a maximum amplitude corresponding to the attachment point of the deflector at the wall. This type of flow was typical of all the baffled tests with the liquid surface initially at the baffle position. In the example shown by Figure 14, a second column of about the same diameter as the first was formed at the opposite tank wall. The second column did not reach an amplitude as great as the first but simply fell across the tank and quickly re-collected with the liquid bulk. The liquid mass contained in both columns was very small compared to the total mass of liquid in the tank.

Presumably, the deflected column is a result of the interaction of the liquid flowing across the top of the baffle and the liquid below the baffle being turned upward and toward the center of the tank by the baffle surface. It is, therefore, suspected that the orientation of the baffle influenced the trajectory of the deflected column.

Liquid Level Below Baffle Position - In the series of tests with the liquid level below the baffle, the predrop slosh amplitudes were less than the distance between the baffle and the nominal liquid level. Therefore, it was possible to measure the liquid amplitude histories before drop and make a quantitative evaluation of the baffle. Measured Froude numbers in these tests ranged from about 0.561 to 11. The measured maximum liquid amplitudes are shown in Figure 13 for comparison with the data from the tests without the baffle. As mentioned previously, at a given Froude number the baffle significantly reduced the maximum amplitude in the low gravity environment.

In general, following the reduction in acceleration, the liquid would "pile up" under the baffle on the side of the tank toward which the surface flow was moving at the time of drop. A small quantity of liquid usually spilled around the lip of the baffle and collected between the top surface of the baffle and the tank wall, where it remained for the duration of the low gravity period. The liquid interface around the remainder of the circumference of the tank spread up the wall due to surface tension and collected under the baffle with some occasional spillage over the lip. Figure 15 shows a comparison of frames from the films of test 2F-41 (no baffle) and 2G-9 (baffle and deflector installed). The fluid motion in the latter test was typical of the flow pattern just described. The Froude number in both cases was about 0.5.

Another type of flow pattern observed was very similar to that described previously, except a column of liquid was formed that had a trajectory toward the center opening of the deflector and a maximum amplitude corresponding approximately to the position of the deflector. Figure 16 shows selected frames from the film of test 2G-6 (baffle and deflector), which exhibited the second type of flow pattern, and test 2F-48 (no baffle). The Froude number in both tests was about 1.3. Based upon the very limited number of tests, the two different flow patterns were not found to be dependent on the Froude number.

In addition to considerably reducing the maximum liquid amplitude, the baffle was also quite effective in damping the fluid oscillations. Figure 17 shows the amplitude histories from tests 2F-41 and 2G-9. In the baffle test, the fluid motion at the wall in the low gravity environment was essentially dissipated after about one second, or about 0.22 times the theoretical low gravity wave period.

In both of the particular liquid-baffle geometries tested, the bulk of the liquid was effectively contained below the baffle following a sudden reduction in applied acceleration. The only liquid above the baffle at any time was either that which spilled over the baffle and became trapped

No Baffles

Baffle and Deflector Installed in Tank

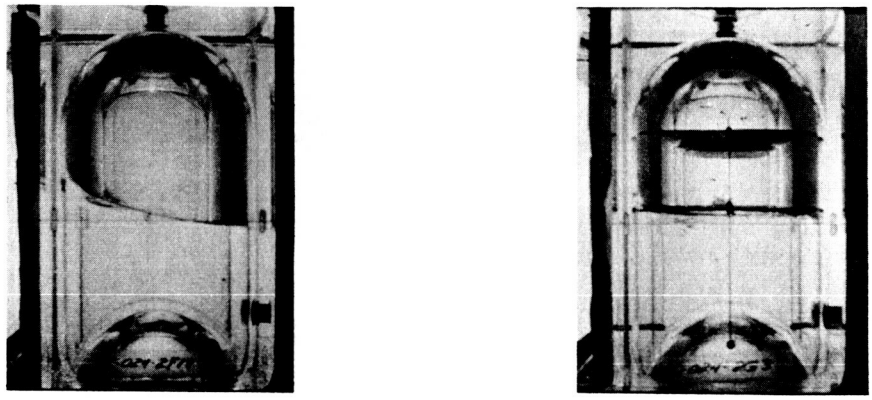

(a) Time = -0.14 seconds (Before Drop)

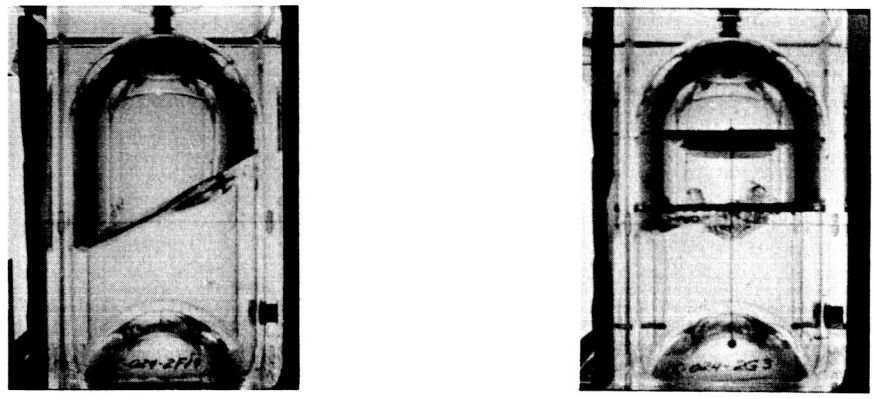

(b) Time = +0.07 seconds (After Drop)

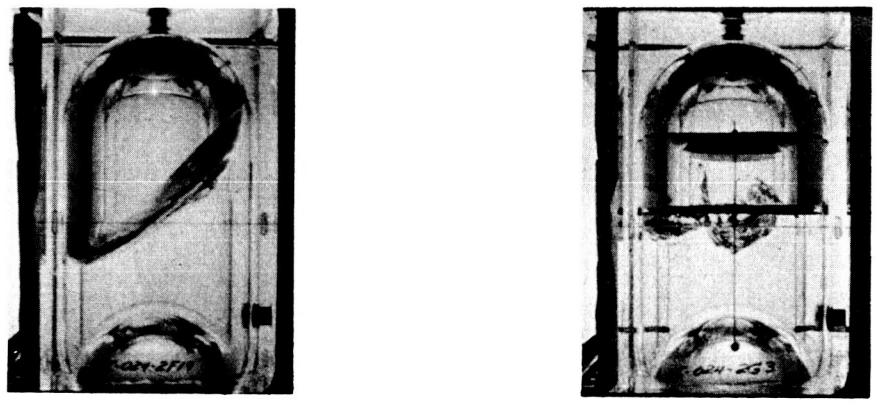

(c) Time = +0.17 seconds

FIG. 14. Effect of AS-203 Baffle and Deflector Configuration on Liquid Behavior with Nominal Liquid Level at the Baffle Position, Froude Number with No Baffle = 14.6

No Baffles

Baffle and Deflector Installed in Tank

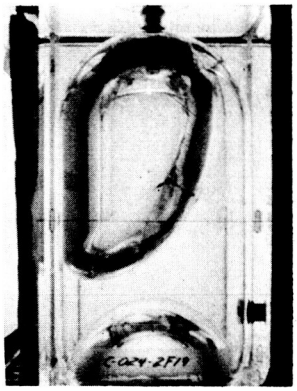

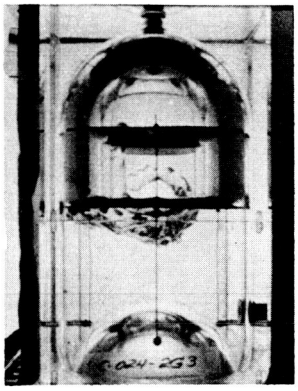

(d) Time = +0.53 seconds

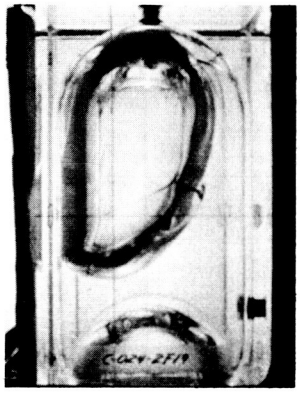

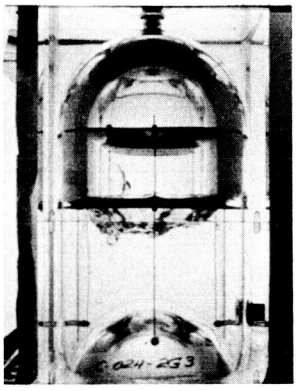

(e) Time = +0.99 seconds

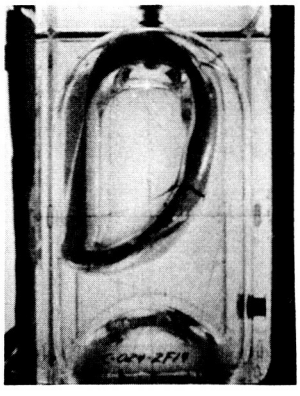

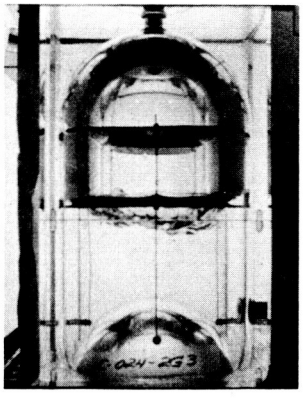

(f) Time = +1.23 seconds

FIG. 14. Effect of AS-203 Baffle and Deflector Configuration on Liquid Behavior with Nominal Liquid Level at the Baffle Position, Froude Number with No Baffle = 14.6 (Continued)

No Baffles

Baffle and Deflector Installed in Tank

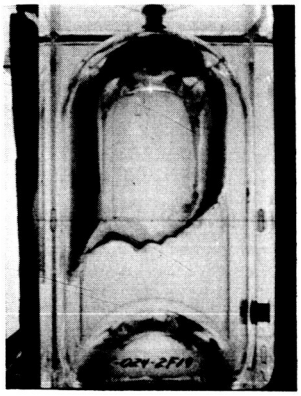

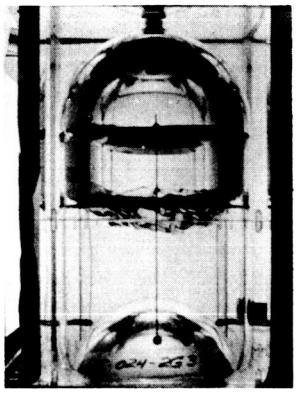

(g) Time = +1.94 seconds

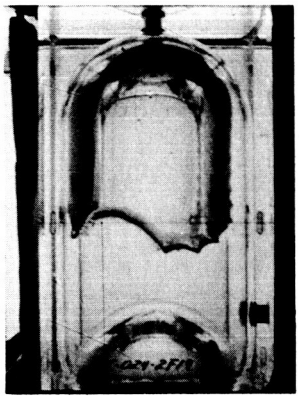

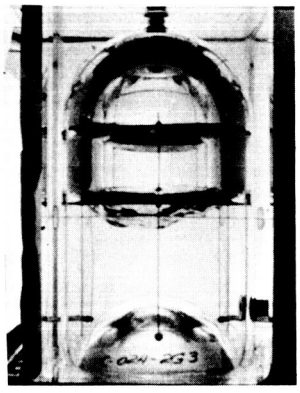

(h) Time = +2.44 seconds

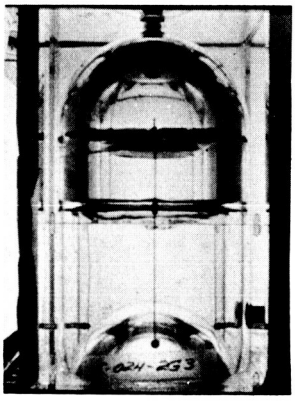

(i) Time = +3.84 seconds

FIG. 14. Effect of AS-203 Baffle and Deflector Configuration on Liquid Behavior with Nominal Liquid Level at the Baffle Position, Froude Number with No Baffle = 14.6 (Concluded)

No Baffles

Baffle and Deflector Installed in Tank

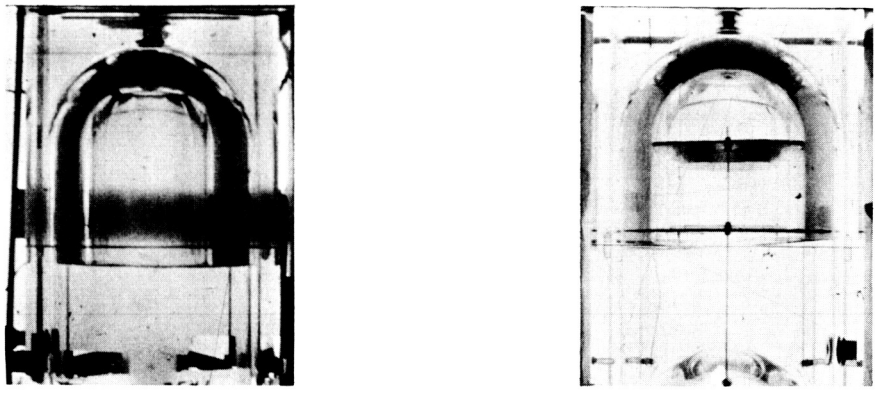

(a) Time = -0.50 seconds (Before Drop)

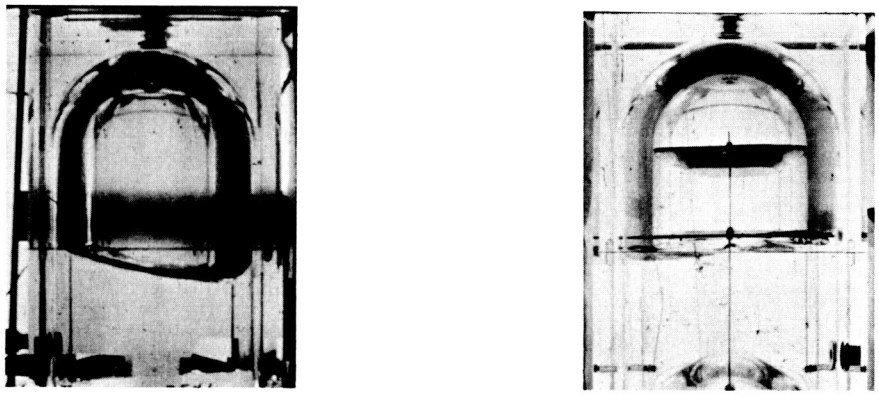

(b) Time = +0.12 seconds (After Drop)

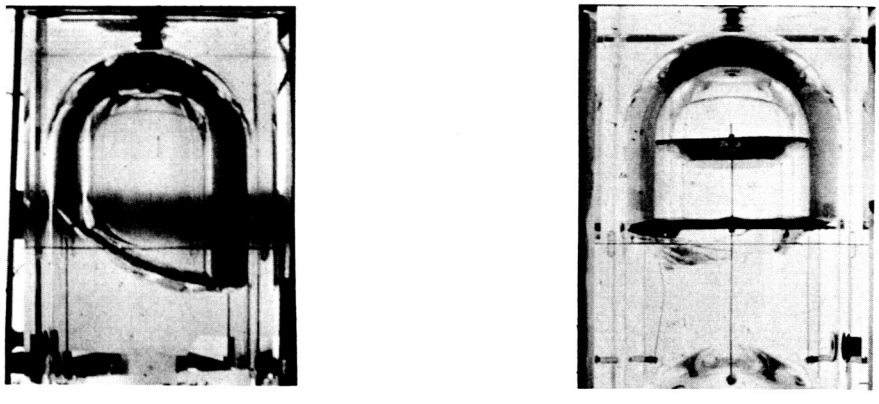

(c) Time = +0.55 seconds

FIG. 15. Effect of AS-203 Baffle and Deflector Configuration on Liquid Behavior with Nominal Liquid Level Below the Baffle Position, Froude Number = 0.5

No Baffles

Baffle and Deflector Installed in Tank

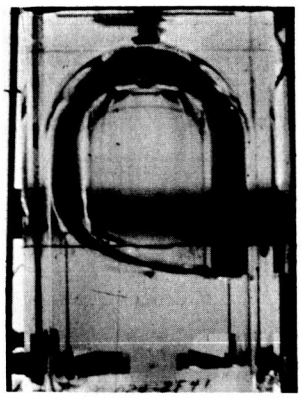

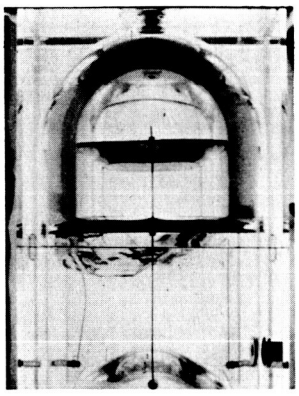

(d) Time = +1.10 seconds

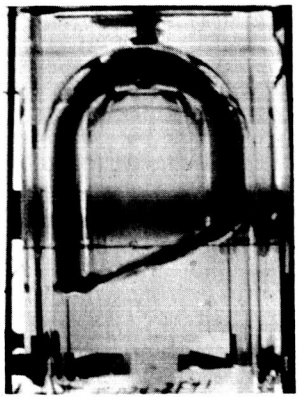

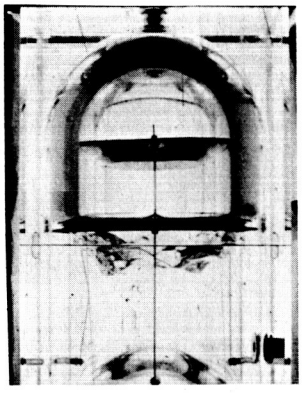

(e) Time = +1.81 seconds

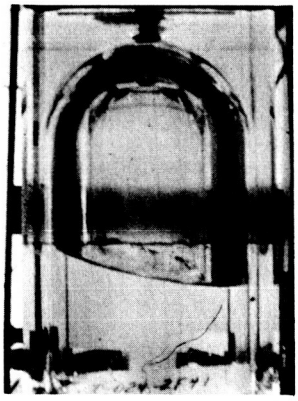

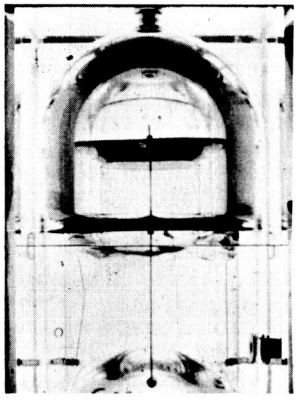

(f) Time = +3.23 seconds

FIG. 15. Effect of AS-203 Baffle and Deflector Configuration on Liquid Behavior with Nominal Liquid Level Below the Baffle Position, Froude Number = 0.5 (Concluded)

No Baffles

Baffle and Deflector Installed in Tank

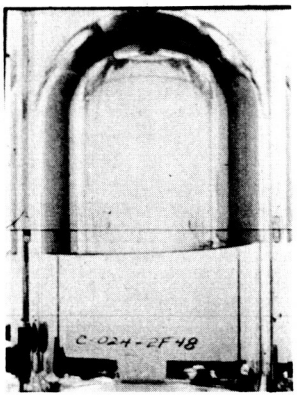

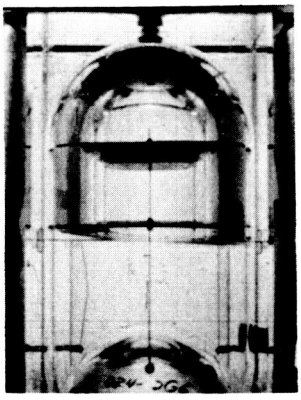

(a) Time = -0.26 seconds (Before Drop)

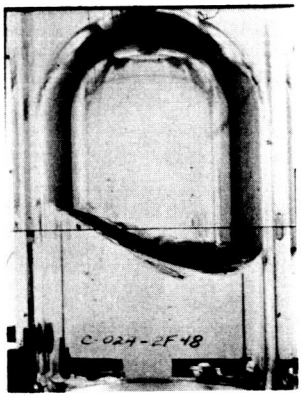

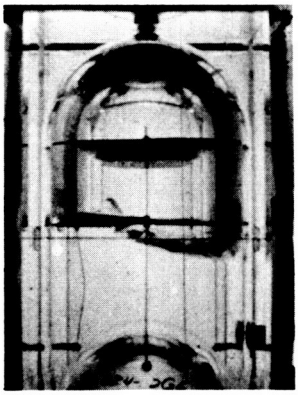

(b) Time = +0.30 seconds (After Drop)

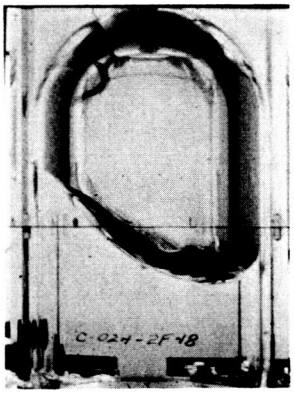

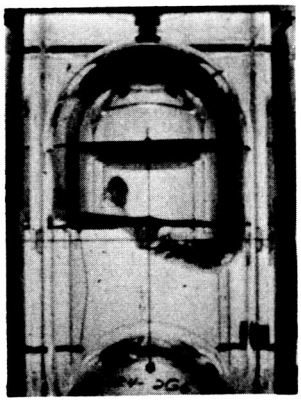

(c) Time = +0.51 seconds

FIG. 16. Effect of AS-203 Baffle and Deflector Configuration on Liquid Behavior with Nominal Liquid Level Below the Baffle Position, Froude Number = 1.3

No Baffles

Baffle and Deflector Installed in Tank

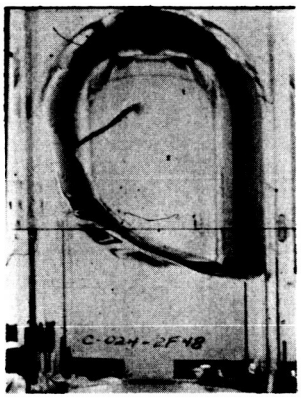

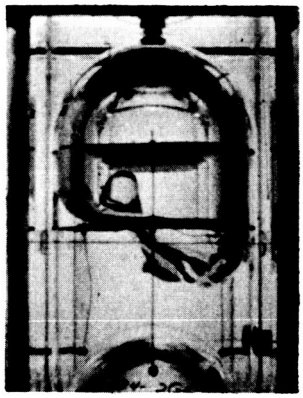

(d) Time = +1.12 seconds

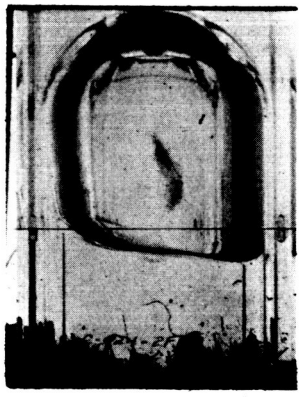

(e) Time = +1.39 seconds

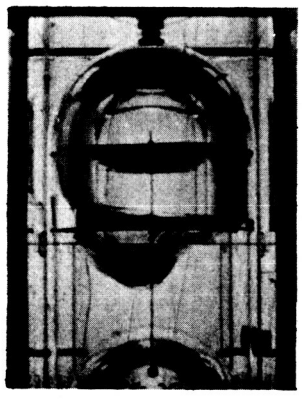

(f) Time = +2.13 seconds

FIG. 16. Effect of AS-203 Baffle and Deflector Configuration on Liquid Behavior with Nominal Liquid Level Below the Baffle Position, Froude Number = 1.3 (Concluded)

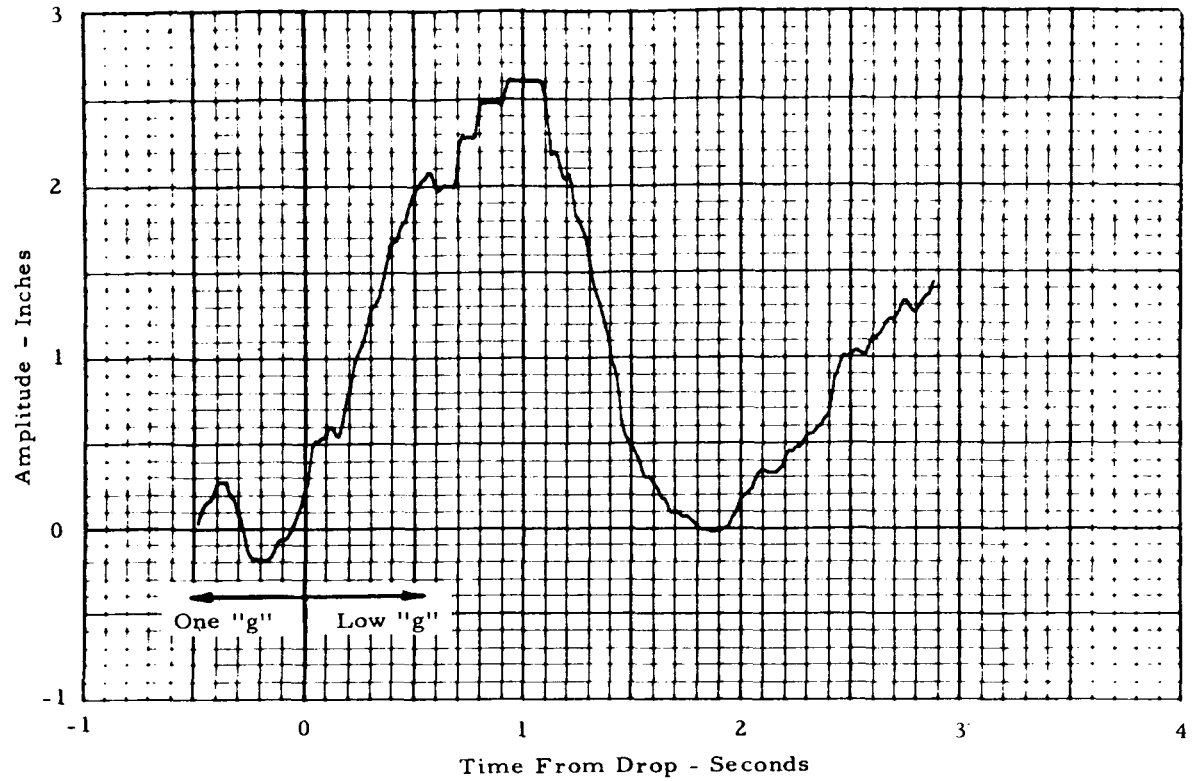

a. No Baffle In Tank (Test 2F-41)

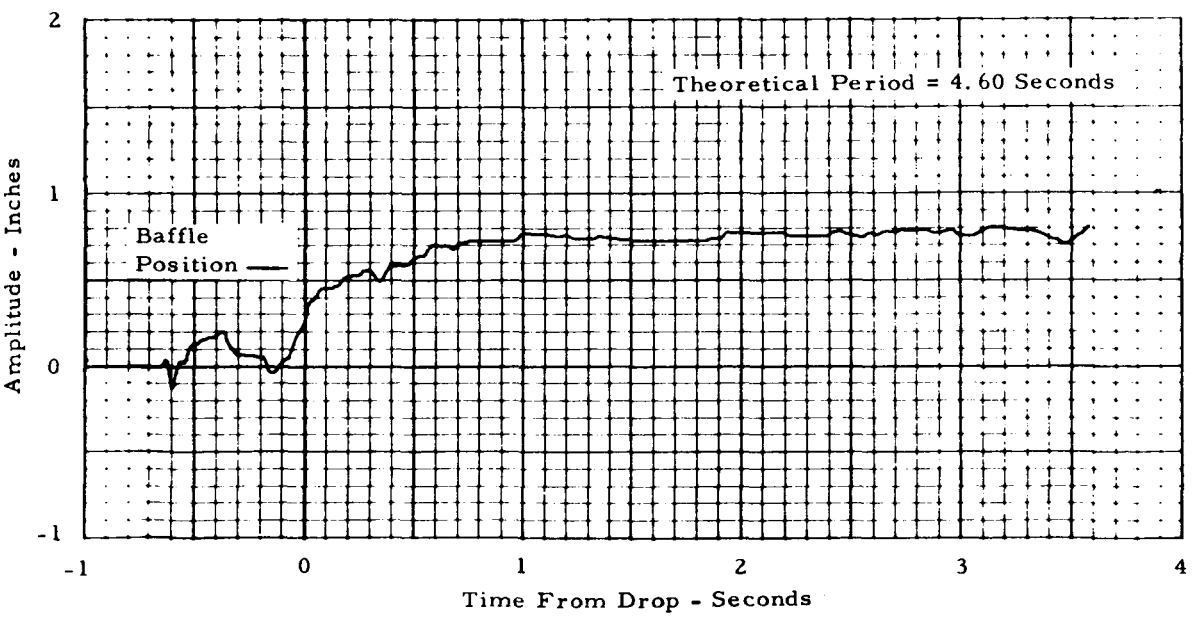

b. S-IVB-203 Baffle and Deflector (Test 2G-9)

FIG. 17 Effect of an Anti-Slosh Baffle on Liquid Amplitude History in a Cylindrical Tank

between the tank wall and the baffle surface and/or the deflected liquid column. In either case, the quantity of liquid above the baffle was insignificant in relation to the total contained mass.

Comparison with AS-203 Flight Results - On the basis of the preceding observations, it was concluded that there should not be a significant liquid hydrogen control problem at orbital insertion of the AS-203 vehicle if the liquid level was within the expected range with respect to the baffle. The results of the AS-203 flight, which occurred on July 5, 1966, substantiated this conclusion. The LH_2 sloshing amplitude and frequency measured during powered flight of the S-IVB stage indicated a maximum possible Froude number at orbital insertion of about 2.3.

The major liquid flow pattern following orbital insertion, as observed by television, appeared to be a movement of the entire liquid surface across the tank. A column of liquid was then observed to enter the field of view and follow a trajectory that carried it diagonally across the tank and toward the forward dome. Portions of the column continued forward through the center opening of the deflector and then broke into smaller fragments that gradually fell back and re-collected with the bulk of the liquid in the bottom of the tank. In general, the observed liquid motion was very similar to the motion observed in the model tests under approximately similar energy conditions (see Figure 16). A more detailed description of the AS-203 flight results is available in Reference 10.

Shifts in Liquid Center of Gravity

The maximum shift in the liquid center of gravity following a reduction in acceleration was determined from the liquid-vapor interface profiles measured at the time the liquid was at its maximum amplitude. In general, as the liquid amplitude increased in the low gravity environment, two distinct interface profiles became apparent. One profile represents the interface in a plane passing through the centerline of the container and perpendicular to the direction of view. The second profile represents the intersection of the liquid-vapor interface with the tank wall. Figure 18 illustrates the typical geometry of these profiles when the liquid is at maximum amplitude and the notation used in the evaluation of the results.

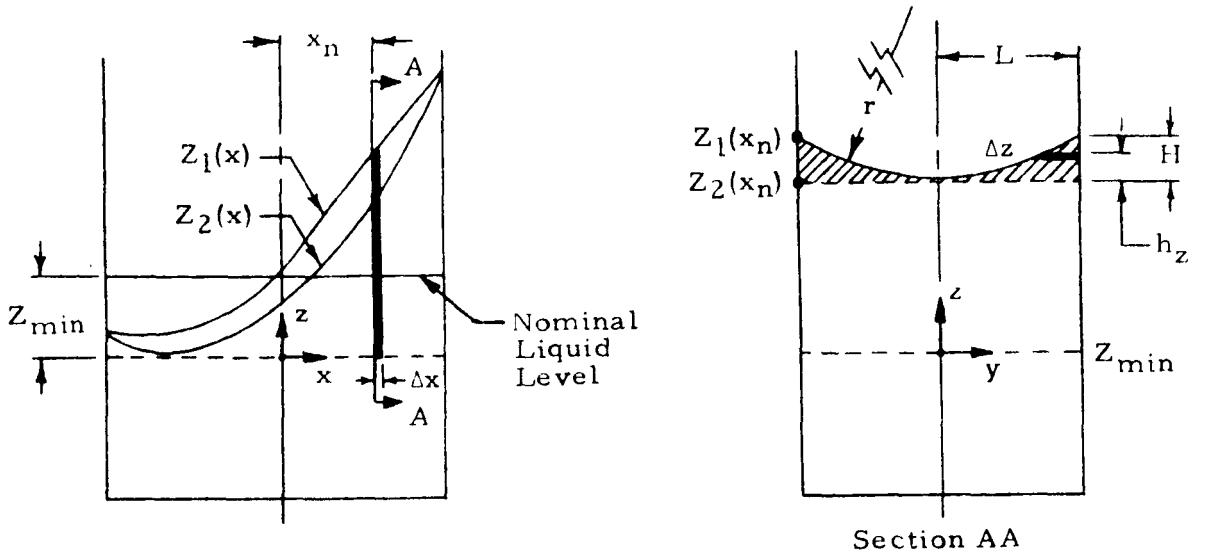

FIG. 18. Nomenclature for Evaluation of Liquid Center of Gravity

To present the results in general form, only those tests were evaluated in which the liquid remained totally on the cylindrical surface of the tank. In addition, the coordinates of the center of gravity were determined only for the liquid volume above the minimum point on the low gravity interface, Z_{min}, when the liquid was at its peak amplitude. The volume in question is the volume bounded by the liquid-vapor interface, the tank wall, and the xy plane. This procedure was used to make the coordinates independent of the liquid depth and the geometry of the bottom of the container. The center of gravity of the liquid above the xy plane can be easily combined with the center of gravity of the liquid below the xy plane to obtain the center of gravity of the entire liquid column for any particular nominal liquid depth. The results should be sufficiently accurate for most engineering purposes so long as $h/R > 1.0$. The dimensionless distance, Z_{min}/R, of the minimum point on the interface below the nominal liquid level is shown as a function of Froude number by Figure 19. As would be expected, Z_{min}/R, increases with increasing Froude number.

The center of gravity of the liquid mass above the xy plane was determined by numerical integration using the following procedure: Let $Z_1(x)$ represent the equation of the upper curve and $Z_2(x)$ represent the equation of the lower curve where $Z_1(x)$ and $Z_2(x)$ were determined from a least squares polynomial curve fit of the measured coordinates of the two curves. The shape of the interface on any cross section, x_n,

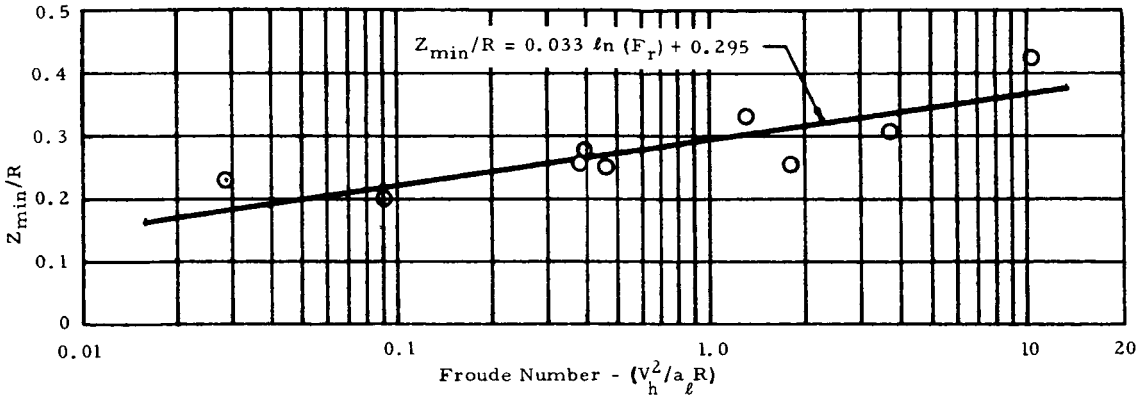

FIG. 19. Maximum Depth of Liquid-Vapor Interface Below Nominal Liquid Level When Liquid is at Peak Amplitude

taken parallel to the direction of view (Section AA of Figure 18) was assumed to be symmetrical and was approximated by a circular arc where the contact angle boundary condition at the wall was neglected. The liquid volume and the moments with respect to the xy and yz planes were calculated for each increment and summed to give the total volume and moments. Finally, the coordinates of the center of gravity referenced from the point defined by the intersection of the tank centerline with the xy plane are,

$$\overline{x} = M_{yz}/v \tag{20}$$

$$\overline{z} = M_{xy}/v \tag{21}$$

A detailed description of the formulation used for evaluating the data is given in the Appendix.

Figure 20 shows the coordinates of the center of gravity of the liquid mass above the xy plane. It is seen that the radial shift in c.g. position, $\overline{x}/R$, is relatively insensitive to Froude number within the range of conditions obtained in these particular tests. The radial coordinate varies from about $\overline{x}/R = 0.39$ at a Froude number of 0.03 to $\overline{x}/R = 0.44$ at a Froude number of 10. The axial coordinate increases with increasing Froude number from a value of $\overline{z}/R = 0.13$ at a Froude number of 0.03 to $\overline{z}/R = 0.27$ at a Froude number of 10.

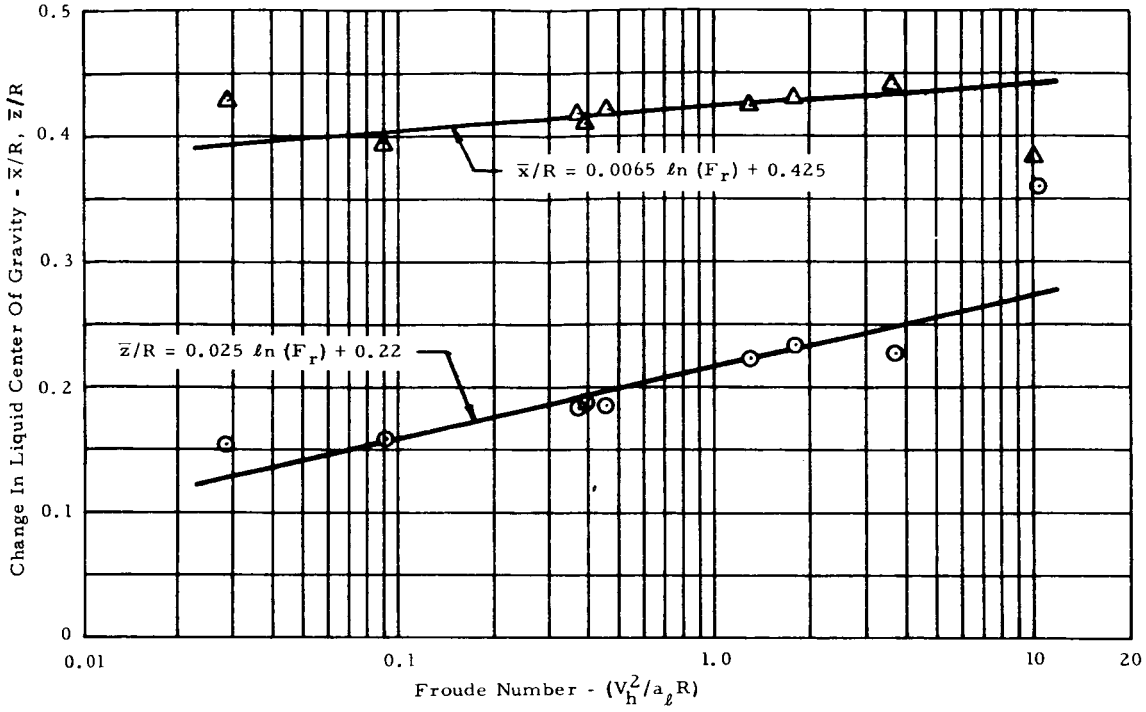

FIG. 20. Coordinates of Liquid Center of Gravity When Liquid-Vapor Interface is at Maximum Amplitude

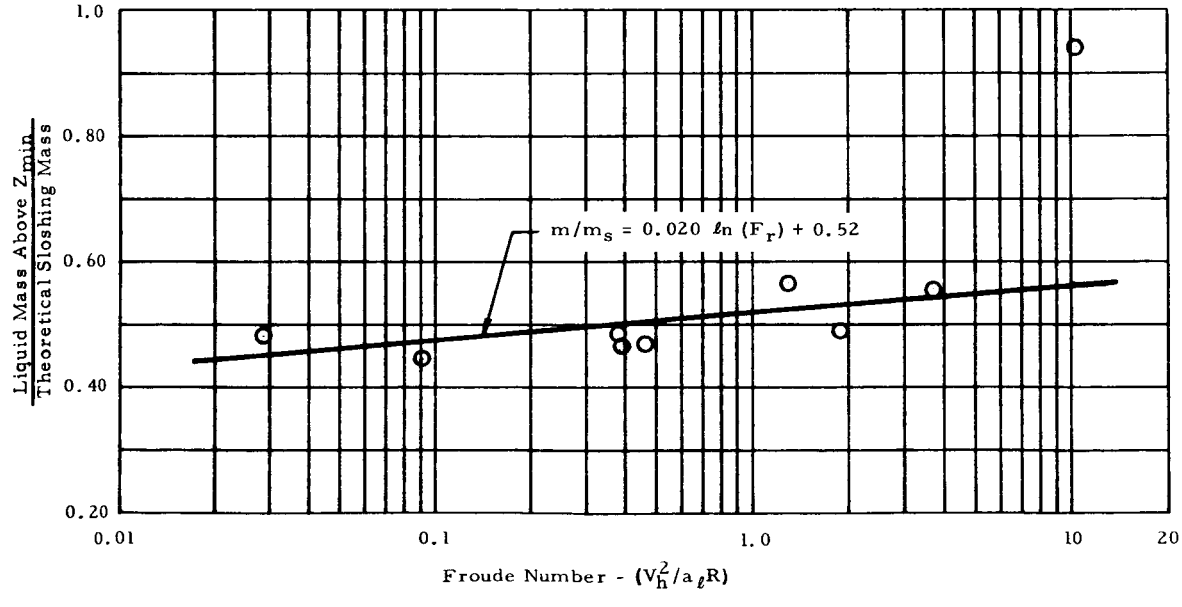

FIG. 21. Ratio of Liquid Mass Above Z_{min} to the Theoretical Sloshing Mass

Figure 21 shows the ratio of the calculated liquid mass above the xy plane to the theoretical sloshing mass as a function of Froude number, where the theoretical sloshing mass is determined from equation (4). The ratio increases from about 0.45 at a Froude number of 0.03 to about 0.56 at a Froude number of 10, based on a best fit curve through the data. Although there is some scatter of the results, the trend is obvious, and the scatter is not particularly bad, considering some of the necessary assumptions used in the analysis.

Time to Reach Maximum Amplitude

The time required for the liquid to first attain its maximum amplitude is of interest with respect to both the attitude control system and the vent system design. This time was determined from the amplitude versus time histories of the various tests and is expressed in the form of the Froude number based on the average velocity of the liquid between the time of release and the time at which the liquid reached its maximum amplitude, that is,

$$F_{ra} = \left(\frac{\Delta\zeta_\ell}{t}\right)^2 / a_\ell R \tag{22}$$

where t is the time in question. Figure 22 shows the Froude number based on the measured average velocity (equation (22)) plotted as a function of the Froude number, based on the measured velocity at release. All values that are shown on both the ordinate and abscissa of Figure 22, except the elapsed time, are known or can be estimated for the particular problem of interest.

For comparative purposes, the theoretical result for uniform linear motion is also shown on the figure. For uniform linear motion, the average velocity over an interval of time is simply,

$$V_a = \frac{V_f + V_i}{2} \tag{23}$$

that is, when the final velocity is zero, the average velocity over the elapsed time interval is one-half of the initial velocity. Substituting $V_i/2$ into equation (22) and dividing the result by the Froude number, based on initial velocity, will show that,

$$F_{ra}/F_r = \frac{V_i^2/4}{a_\ell R} \Big/ \frac{V_i^2}{a_\ell R} \quad \text{or} \quad F_{ra} = F_r/4 \tag{24}$$

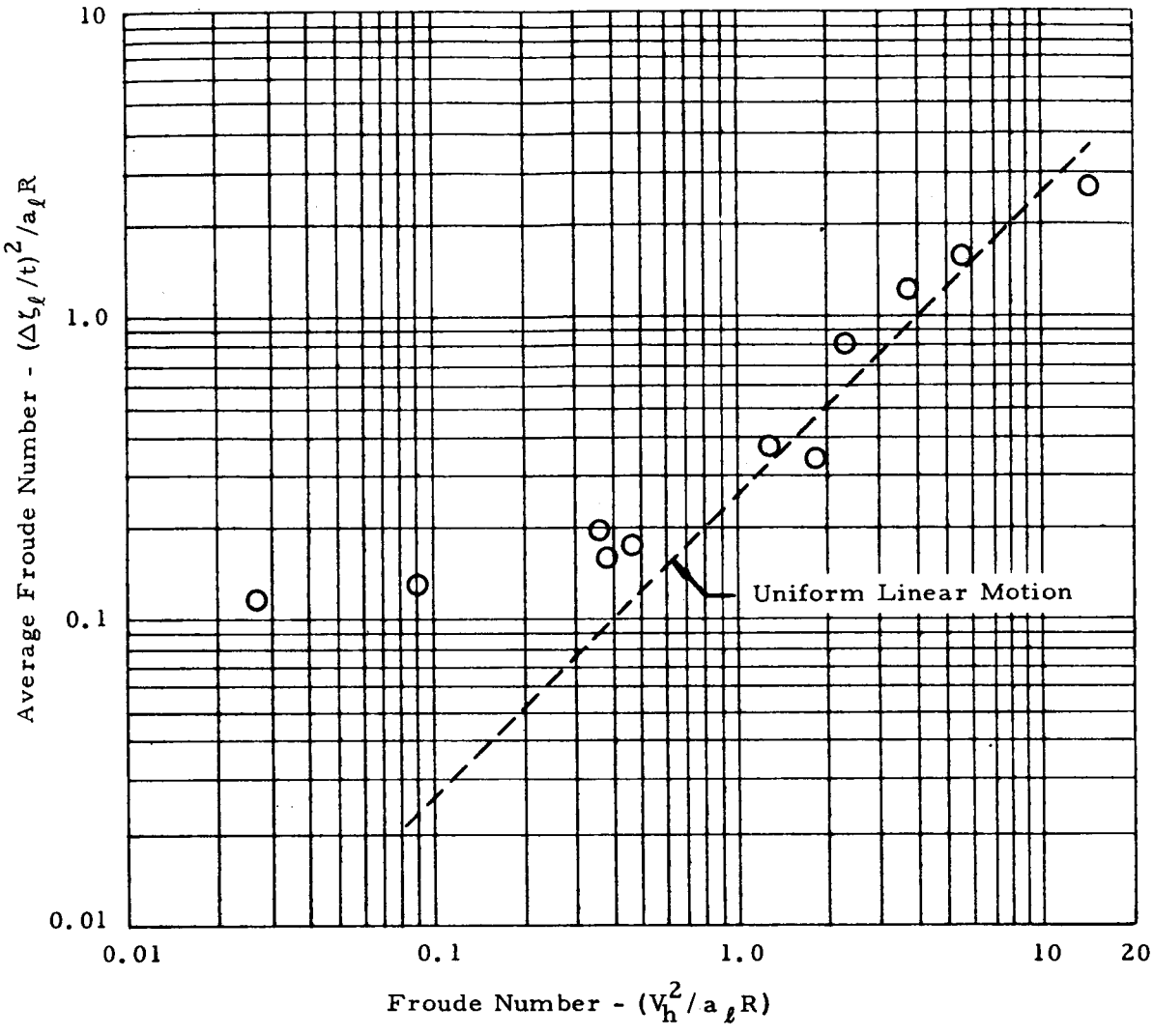

FIG. 22. Elapsed Time After Drop Until Liquid Reaches Maximum Amplitude

From Figure 22 it is seen that at Froude numbers greater than one the measured data generally agree closely with the theory for uniform linear motion. At Froude numbers less than one, the relatively few data points available indicate that the time for the liquid to reach its maximum amplitude is shorter than the time corresponding to uniform linear motion.

Damping of Liquid Oscillations

The test conditions used permitted no more than one complete cycle of motion under the low gravity environment to be observed. However, there were several tests in which two peak amplitudes occurred on one side of the container. From these selected tests it was possible to obtain an indication of the damping characteristics by observing the decreasing amplitude of the liquid oscillation. The test conditions include initial amplitudes of 0.6R to 1.06R, Bond numbers from 57 to 95, and a nearly constant damping parameter of 5×10^{-3}. For each applicable test the peak liquid amplitude measured at half-cycle intervals provided three data points for establishing the logarithmic decrement (equation (10)).

The experimental decrements and values calculated from the empirical equations of Stephens (equation (16)) and Salzman (equation (15)) are shown in Figure 23. In each case, the damping parameter has been computed using the natural frequency determined from equation (6). Since Stephens equation is valid only for large Bond numbers, and Salzman's equation is valid only for zero or near zero Bond numbers, the logarithmic decrement for small amplitude oscillations and Bond numbers within the range of these tests should lie somewhere between the two. As shown, the measured damping is considerably greater than even Salzman's correlation would predict.

The significantly higher logarithmic decrements are apparently a function of the very large sloshing amplitudes. The logarithmic decrement is shown plotted as a function of the initial low gravity sloshing amplitude ratio in Figure 24. The figure clearly illustrates that the damping decrement increases with increasing amplitude when the sloshing amplitude is large. The best fit line through the data, when extrapolated to the lower amplitudes for which most available correlations are applicable, yields values corresponding approximately to those computed from Salzman's equation.

From the limited results of this study, it was not possible to establish an empirical relationship for the effect of Bond number on damping. It was shown, however, that if a sudden reduction in acceleration produces large amplitude sloshing, the initial damping will be quite high.

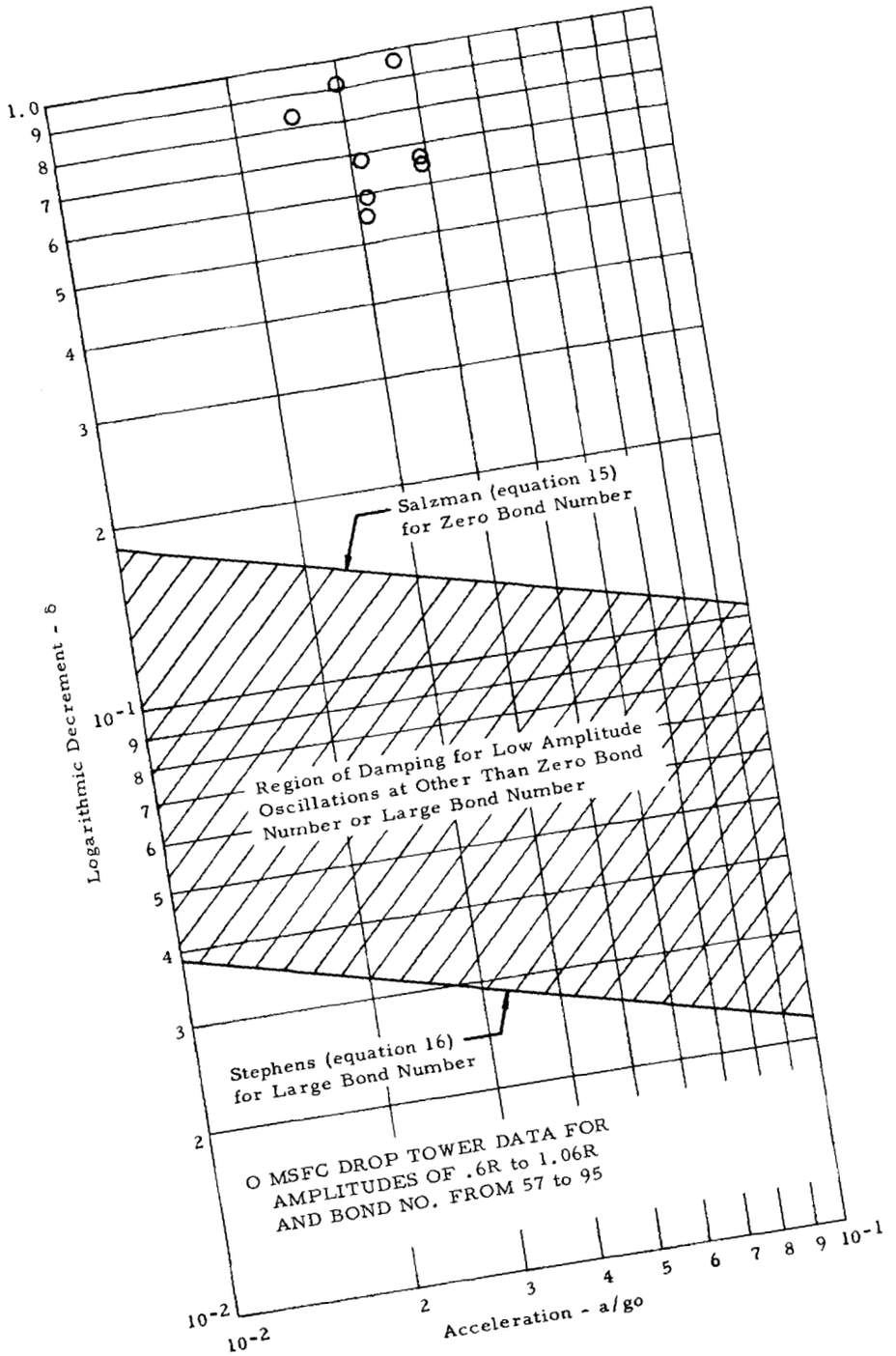

FIG. 23. Damping of Free Surface Oscillations Under Reduced Gravity Conditions

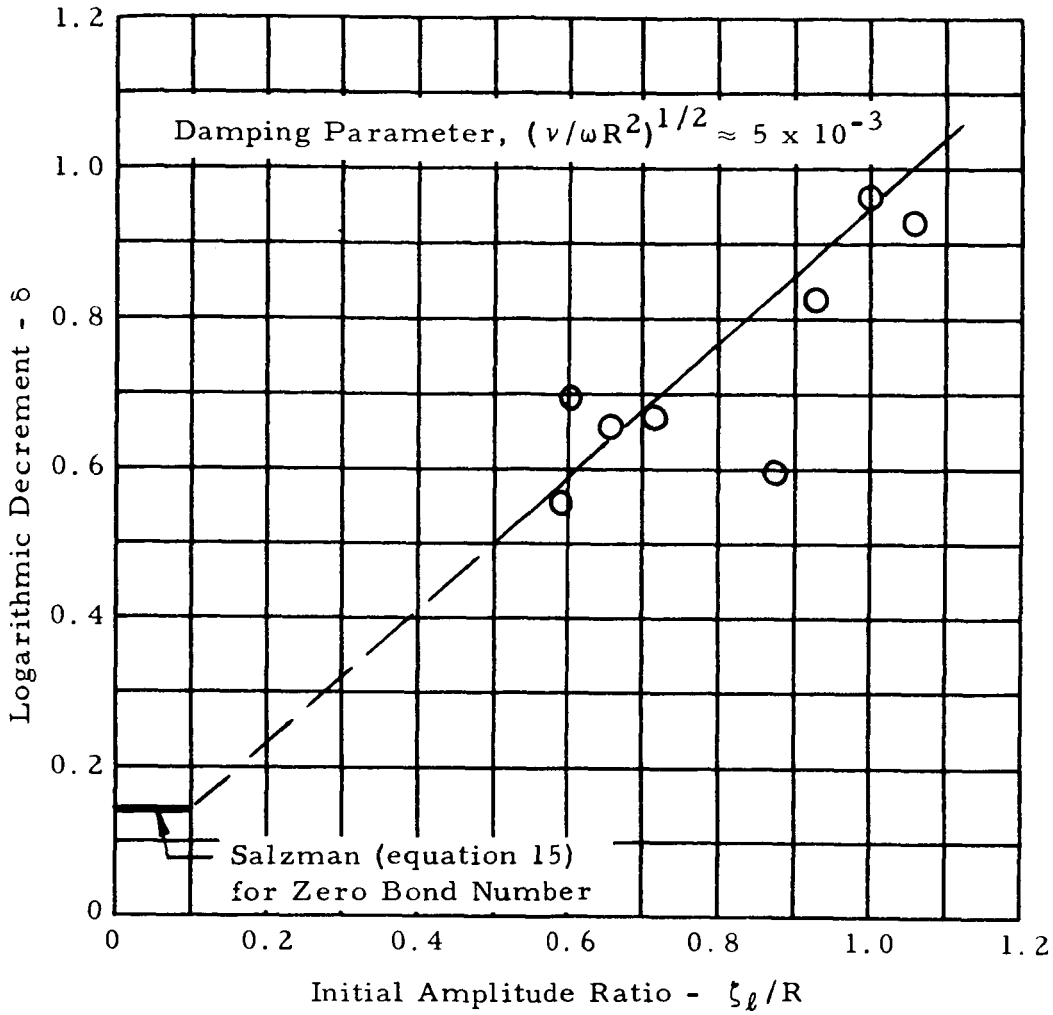

FIG. 24. Variation of the Logarithmic Decrement with Initial Amplitude Ratio

Period of Oscillation

The period of oscillation of the liquid column under reduced gravity conditions was evaluated from the amplitude-time traces of the various tests by measuring, along any suitable horizontal axis, the time required to complete one full cycle of motion. Figure 25 shows three typical amplitude-time traces to illustrate the method used to determine the wave period. Whenever possible, the wave period was measured along the zero axis (quiescent flat liquid surface) as shown by Figure 25a. In some cases a complete cycle could not be measured along the zero axis. However, in most tests it was possible to choose

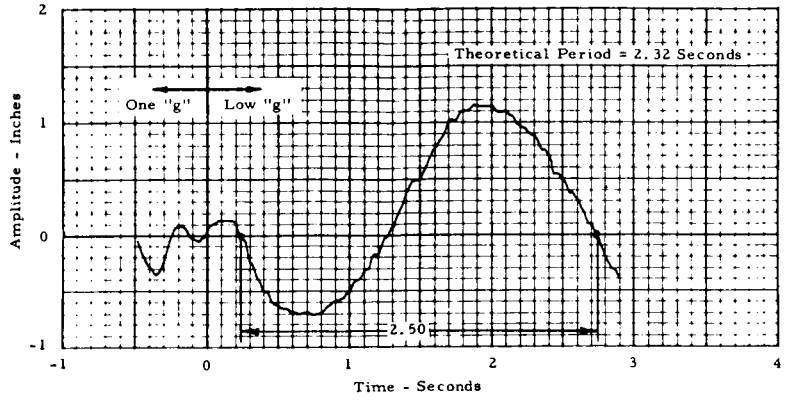

(a) Test 2F-42, Right Side Wall

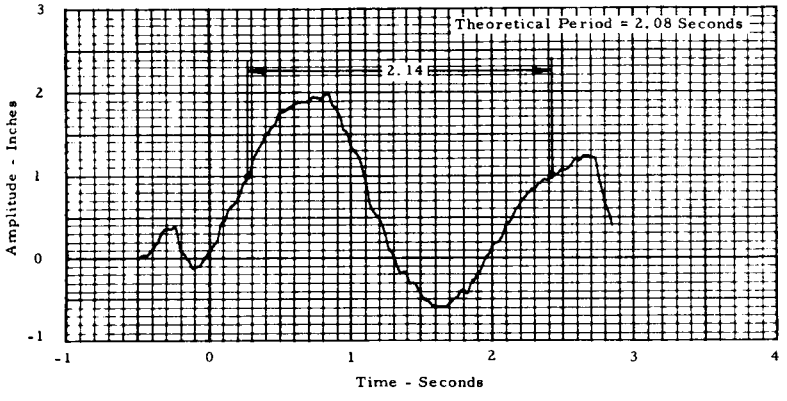

(b) Test 2F-49, Left Side Wall

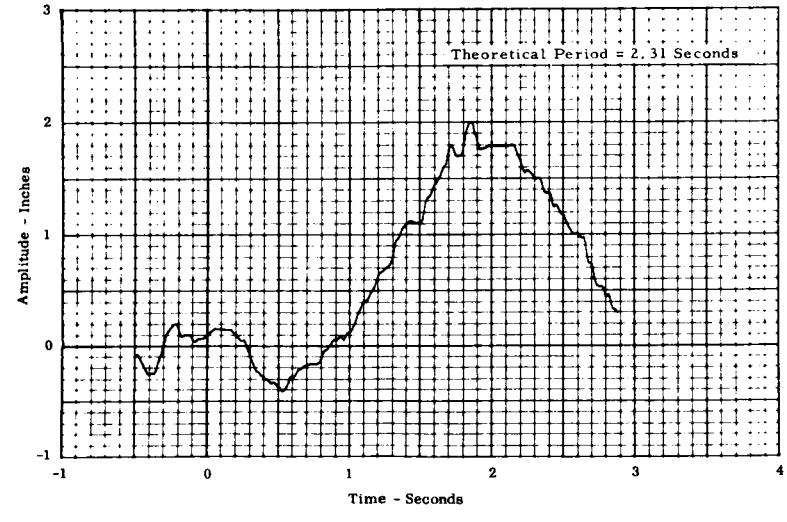

(c) Test 2F-41, Right Side Wall

FIG. 25. Typical Amplitude-Time Histories Showing Method of Measuring Wave Period During Low Gravity Tests

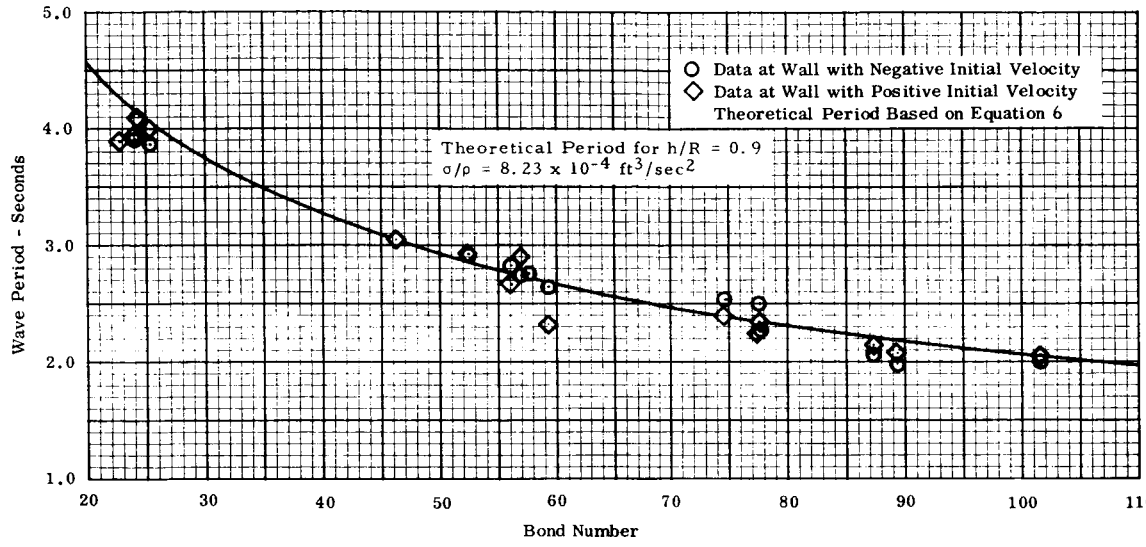

FIG. 26. Measured Wave Period as a Function of Bond Number

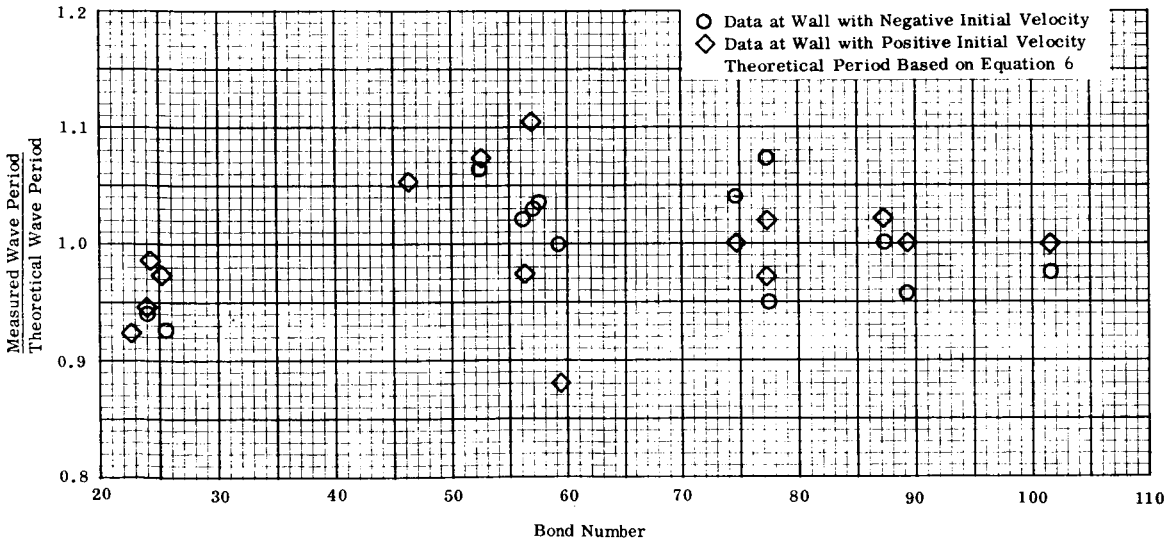

FIG. 27. Ratio of Measured Wave Period To Theoretical Wave Period at Various Bond Numbers

some other axis along which a full cycle could be measured. Figure 25b illustrates a case in which the +1.0 axis was used for reference. No attempts were made to measure wave periods from the tests in which no suitable axis could be established. An example of such a case is shown in Figure 25c.

The measured wave periods as a function of Bond number are shown in Figure 26. Also shown is the theoretical wave period as determined from the Satterlee-Reynolds equation (6) for $h/R = 0.9$ and a kinematic surface tension of $8.23 \times 10^{-4}\ ft^3/sec^2$, which is the median value of surface tension based upon the fluid temperatures measured during the various tests. A more accurate comparison of the measured and theoretical wave periods is given by Figure 27, which shows the ratio of the measured period to the theoretical period plotted as a function of Bond number. In this case, the theoretical period was computed from the actual filling height and kinematic surface tension for each test. With two exceptions, the measured periods are within 8 percent of the theoretical period, and the maximum deviation from the theoretical period is only 12 percent. Furthermore, the data appear to scatter uniformly about the theoretical value at all Bond numbers tested. That is, there is no obvious tendency for the measured wave period to deviate significantly from the Satterlee-Reynolds equation at either low or high Bond numbers. Since the experimental wave periods were measured from the first complete cycle of motion under the reduced gravity environment and these measured data agree so closely with the theoretical period, it is concluded that, for all practical purposes, the liquid column shifts frequency instantaneously with changes in apparent gravitational field.

CONCLUSIONS

The results of this study indicate that, for Froude numbers from about 0.03 to 14 in combination with Bond numbers from 24 to 100, the maximum amplitude of a fundamental mode antisymmetric slosh wave following a sudden reduction in acceleration is uniquely dependent on the Froude number and increases with increasing Froude number according to the expression

$$\Delta\zeta_\ell / R = 0.99\ (F_r)^{[0.018\ \ell n(F_r) + 0.177]}$$

The energy conditions predicted to exist in the S-IVB-203 LH_2 tank at orbital insertion without the baffle and deflector in the tank (Froude number = 19.3) were sufficient to produce amplification of the slosh wave to the top of the model tank forward dome for at least two successive cycles of motion in the low gravity environment. Over the range of Froude numbers studied, the corresponding amplitudes in unbaffled tanks were generally such that the use of auxiliary devices for reducing the propellant motions should be considered in practical applications.

A single ring baffle with a width-to-tank radius ratio of 0.16, positioned either at or slightly above the nominal liquid surface, was highly effective in reducing slosh wave amplification and damping the low gravity liquid motion. Although baffles are not normally required in upper stage vehicles for purposes of guidance and control during powered flight, they have definite merit for low gravity propellant control.

The general nature of the liquid behavior in model tests using an S-IVB-203 baffle and deflector configuration was very similar to that observed in the LH_2 tank of the AS-203 vehicle immediately following orbital insertion.

In an unbaffled tank, the maximum center of gravity shift, which occurred when the liquid was at its peak amplitude, increased in both the radial and axial directions with increasing Froude number. For liquid depths, $h/R \gtrsim 1.0$, the radial coordinate of the center of gravity of the liquid mass above the lowest point on the liquid-vapor interface is determined from the expression, $\overline{x}/R = 0.0065\, \ell n\, (F_r) + 0.425$. The axial coordinate is given by $\overline{z}/R = 0.025\, \ell n(F_r) + 0.22$ where the point of reference of $\overline{x}$ and $\overline{z}$ is defined by Figure 18.

The time required for the liquid to attain its maximum amplitude was found to be dependent on the Froude number. At Froude numbers greater than 1.0 the measured time agreed well with the time corresponding to uniform linear motion.

When large amplitude sloshing occurs in a low gravity environment, the initial natural damping is considerably higher than predicted by available damping correlations. The logarithmic decrement exhibits an apparent amplitude dependence, increasing with increasing amplitude.

For all practical purposes, the frequency of oscillation of the liquid column shifts instantaneously with changes in the applied acceleration. The measured wave period of the first cycle of motion following a reduction in acceleration agrees with the Satterlee-Reynolds equation within ± 8 percent at all Bond numbers within the range 24 to 100.

APPENDIX

DESCRIPTION OF EQUATIONS FOR CALCULATING LIQUID CENTER OF GRAVITY

The maximum shift in the liquid center of gravity following a reduction in acceleration has been determined from the liquid-vapor interface profiles measured at the time the liquid was at its maximum amplitude. In general, as the liquid amplitude increased in the low gravity environment, two distinct interface profiles became apparent. One profile is that which represents the interface in a plane passing through the centerline of the container and perpendicular to the direction of view. The second profile is that which represents the intersection of the liquid-vapor interface with the tank wall as the liquid rises and spreads around the wall into and away from the line of sight due to surface tension. Figure 18 illustrates the typical geometry of these profiles at maximum amplitude and indicates the notation used in the evaluation of the results. The following procedure was used to evaluate the test results.

Let $Z_1(x)$ represent the equation of the upper curve and $Z_2(x)$ represent the equation of the lower curve, where $Z_1(x)$ and $Z_2(x)$ were determined from a least squares polynomial curve fit of the measured coordinates of the two curves. The shape of the interface on any cross section, x_n, taken parallel to the direction of view was assumed to be symmetrical and was approximated by a circular arc where the contact angle boundary condition at the wall was neglected. The depth, H, of the circular section was evaluated as,

$$H = Z_1(x_n) - Z_2(x_n) \tag{A1}$$

and the semi-chord length of the circular arc is

$$L = (3^2 - x_n^2)^{\frac{1}{2}} \tag{A2}$$

The radius, r, of the circular section is,

$$r = (H^2 + L^2)/2H \tag{A3}$$

The volume of the crosshatched area of thickness, Δx, shown in Section AA of Figure 18 is,

$$\Delta v_s = \{2LH - r^2 \tan^{-1}[L/(r-H)] - (r - H)L\}\Delta x \tag{A4}$$

and the volume of the rectangular section between Z_{min} and $Z_2(x_n)$ is simply

$$\Delta v_R = 2L[Z_2(x_n) - Z_{min}]\Delta x \tag{A5}$$

The total liquid volume above the xy plane

$$v = \sum_{n=1}^{N} (\Delta v_s + \Delta v_R) \tag{A6}$$

Summing the moments of the Δz elements from Z_2 to Z_1 provides the contribution of the cross hatched volume of the section at x_n to the total moment with respect to the xy plane.

$$(\Delta M_{xy})_s = \{\Sigma 2[(Z_2 - Z_{min}) + h_z][L - (2rh_z - h_z^2)^{\frac{1}{2}}]\Delta z\}\Delta x \tag{A7}$$

The moment of the rectangular volume with respect to the xy plane is,

$$(\Delta M_{xy})_R = L[Z_2(x_n) - Z_{min}]^2 \Delta x \tag{A8}$$

The moment of the entire liquid section at x_n with respect to the xy plane is,

$$\Delta M_{xy} = (\Delta M_{xy})_s + (\Delta M_{xy})_R \tag{A9}$$

The moment of the section with respect to the yz plane is,

$$\Delta M_{yz} = x_n(\Delta v_s + \Delta v_R) \tag{A10}$$

The total moment with respect to the xy plane becomes,

$$M_{xy} = \sum_{n=1}^{N} (\Delta M_{xy}) \tag{A11}$$

and the total moment with respect to the yz plane is,

$$M_{yz} = \sum_{n=1}^{N} (\Delta M_{yz}) \tag{A12}$$

Finally, the coordinates of the center of gravity referenced from the point defined by the intersection of the tank centerline with the xy plane are,

$$\bar{x} = M_{yz}/v \tag{A13}$$

$$\bar{z} = M_{xy}/v \tag{A14}$$

REFERENCES

1. Results of the Seventh Saturn I Launch Vehicle Test Flight (SA-7), MSFC Document MPR-SAT-FE-64-17, November 25, 1964.

2. Satterlee, H. M.; and Reynolds, W. C.: The Dynamics of the Free Liquid Surface in Cylindrical Containers Under Strong Capillary and Weak Gravity Conditions, Stanford University Technical Report LG-2, May 1, 1964.

3. Stephens, D. G.; Leonard, H. W.; and Perry, T. W.: Investigation of the Damping of Liquids in Right Circular Cylindrical Tanks, Including the Effects of a Time-Variant Liquid Depth, NASA TND-1367, July 1962.

4. Abramson, H. N.: The Dynamic Behavior of Liquids in Moving Containers, NASA SP-106, 1966.

5. Salzman, J. A.; Labus, T. L.; and Masica, W. J.: An Experimental Investigation of the Frequency and Viscous Damping of Liquids During Weightlessness, NASA TN D-4132, August 1967.

6. McAnelly, W. B.; and Covington, S.S.: Low Gravity Fluid Mechanics Drop Tower Facility, NASA TMX-53765.

7. Bradley, Dale; and Vaughn, John E.: Simulation of a Facility for Zero and Low Gravity Environments, Chrysler Corporation Technical Report HSM-R32-67, May 1, 1967.

8. Fung, F. C. W.: Dynamic Response of Liquids in Partially Filled Containers Suddenly Experiencing Weightlessness, Paper Presented at Symposium on Fluid Mechanics and Heat Transfer Under Low Gravitational Conditions, Palo Alto, California, June 1965.

9. Siegert, C. E.; Petrash, D. A.; and Otto, E. W.: Time Response of Liquid-Vapor Interface After Entering Weightlessness, NASA TND-2458, August 1964.

10. Evaluation of AS-203 Low Gravity Orbital Experiment, Chrysler Corporation Technical Report HSM-R421-67, January 13, 1967.

APPROVAL TM X-53755

AN EXPERIMENTAL STUDY OF THE BEHAVIOR OF A SLOSHING LIQUID SUBJECTED TO A SUDDEN REDUCTION IN ACCELERATION

By Louis E. Toole and Leon J. Hastings

The information in this report has been reviewed for security classification. Review of any information concerning Department of Defense or Atomic Energy Commission programs has been made by the MSFC Security Classification Officer. This report, in its entirety, has been determined to be unclassified.

This document has also been reviewed and approved for technical accuracy.

A. L. WORLUND
Chief, Fluid Mechanics Section

C. C. WOOD
Chief, Fluid-Thermal Systems Branch

H. G. PAUL
Chief, Propulsion Division

W. R. LUCAS
Director, Propulsion and Vehicle Engineering Laboratory

DISTRIBUTION

DIR	Dr. von Braun
DEP-T	Dr. Rees
I-DIR	General O'Connor
	Dr. Mrazek
R-DIR	Mr. Weidner
R-AS-DIR	Mr. Williams
R-RP-DIR	Dr. Stuhlinger
R-AERO-DIR	Dr. Geissler
R-AERO-DD	Mr. Ryan
	Mr. Buchanan
R-COMP-RRT	Mr. Craft (3)
R-TEST-DIR	Mr. Heimburg
R-TEST-B	Mr. Marsalis
R-TEST-BD	Mr. Chumley
R-TEST-BDM	Mr. Simmons
R-TEST-BDS	Mr. Childers
	Mr. Buckelew
R-TEST-C	Mr. Grafton
R-TEST-CT	Mr. Perry
	Mr. Goetz
	Mr. Stone (5)
R-TEST-I	Dr. Sieber
R-TEST-IE	Mr. Shirey
R-TEST-IEM	Mr. Baldwin
R-TEST-II	Mr. Kastanakis
R-TEST-IID	Mr. Proffitt
R-TEST-IIM	Mr. Powell
R-P&VE-DIR	Dr. Lucas
	Mr. Hellebrand
R-P&VE-A	Mr. Goerner
R-P&VE-P	Mr. Paul
	Mr. Isbell
	Mr. Beduerftig
R-P&VE-PA	Mr. Johnson
R-P&VE-PE	Dr. Head
R-P&VE-PP	Mr. Swalley
R-P&VE-PM	Mr. Fuhrmann
	Mr. Voss
R-P&VE-PT	Mr. Wood (5)
	Mr. Worlund
	Mr. Hastings (15)

DISTRIBUTION (Continued)

R-P&VE-PT
Mr. Hopson
Mr. McAnelly
Mr. Vaniman
R-P&VE-RM
Miss Scott
CC-P
I-RM-M
MS-H
MS-IP
MS-IL (8)
MS-T (6)

Scientific and Technical Information Facility (25)
Attn: NASA Representative (S-AK/RKT)
P. O. Box 33
College Park, Maryland 20740

Brown Engineering, A Teledyne Co.
Huntsville, Alabama
Mr. Jarrett, MS-166
Mr. Meyers, MS-166
Mr. Woods, MS-190
Mr. Payne, MS-190

Chrysler Corporation, Space Division
Huntsville, Alabama
Mr. Toole
Mr. Kavanaugh
Mr. Cannizzo
Mr. Messner
Mr. Ziemke

McDonnell Douglas Corporation
MDC - Huntsville, Alabama
Bldg. 4481
Attn: Mr. S. L. Zukerman (3)

Lewis Research Center
21000 Brook Park Rd.
Cleveland, Ohio 44135
Attn: Mr. E. Otto
Mr. D. Petrash

DISTRIBUTION (Concluded)

Manned Spacecraft Center
NASA
Houston, Texas 77058
Attn: J. G. Thibodaux, Chief
Propulsion and Power Division

General Dynamics
P.O. Box 1128
Sandiego, California 92112
Attn: R. E. Tatro (3)
Mail Zone: 584-00

Martin - Marietta Corporation
Denver, Colorado 80201
Attn: Mr. Howard Paynter
Propulsion Research Department

NASA Headquarters
600 Independence Ave., S. W.
Washington, D. C. 20546
Attn: Mr. J. A. Suddreth (3)
Code RPL
Liquid Propulsion Technology